https://doi.org/10.5194/egusphere-2026-1669
Preprint. Discussion started: 12 May 2026

Tracking organic compounds in smoke plumes using infrared satellite-based measurements

Julieta F. Juncosa Calahorrano[1], Dylan B. Millet[1], Kelley C. Wells[1], Chengyuan Hu[1], Jared F. Brewer[1], Vivienne H. Payne[2], Wade Permar[3], Lu Hu[3], Amy P. Sullivan[4], I-Ting Ku[4], Emily V. Fischer[4], Vanessa Selimovic[5], Kanako Sekimoto[6], Aaron Lamplugh[7], Georgios Gkatzelis[8], Jessica B. Gilman[9], Matthew Coggon[9], Carsten Warneke[9].

[1]Department of Soil, Water and Climate, University of Minnesota, Minneapolis, MN 55108, USA.
[2]Jet Propulsion Laboratory, California Institute of Technology. Pasadena, CA, 91011, USA.
[3]Department of Chemistry and Biochemistry, University of Montana, Missoula, MT, 59812, USA.
[4]Department of Atmospheric Science, Colorado State University, Fort Collins, CO, 80521, USA.
[5]Department of Chemistry, University of Michigan, Ann Arbor, MI, 48109, USA
[6]Graduate School of Nanobioscience,Yokohama City University, Yokohama, Kanagawa Prefecture, Japan
[7]Colorado Department of Public Health and Environment (CDPHE), Denver, CO, 80246, USA
[8]Institute of Climate and Energy Systems, ICE-3: Troposphere, Forschungszentrum Jülich GmbH, Jülich 52428, Germany
[9]National Oceanic and Atmospheric Administration, Chemical Science Laboratory, Boulder, CO, 80305, USA.

Correspondence to: Dylan B. Millet (dbm@umn.ude)

Abstract

We apply new measurements of methanol, ethene, ethyne, and HCN from the Cross-track Infrared Sounder (CrIS) to explore the quantitative use of satellite-based thermal infrared (IR) observations for fire studies. We focus analysis on the western U.S. during the 2018-2019 timeframes of two fire-focused aircraft campaigns, and use the GEOS-Chem model to guide interpretation. The CrIS data reveal large in-smoke enhancements and species:species correlations for targeted volatile organic compounds (VOCs), especially during the more active

2018 fire year. Spectral enhancements are strongest for methanol and ethene. For VOCs with similar vertical sensitivities the in-smoke correlations are height-independent and can be converted to column enhancement ratios without plume altitude information. For VOCs with dissimilar vertical sensitivities, spectral index correlations change coherently with altitude and may constrain injection or plume height changes. The mean (± σ) ethene:methanol ratio measured by CrIS across an ensemble of plumes (0.64 ± 0.24 mol/mol) matches bottom-up emission ratios (0.63 ± 0.08 mol/mol), but satellite-based and aircraft data both reveal greater variability than is predicted by GEOS-Chem. We propose that fire pyrolysis conditions are one driver of this variability and use in-situ data to show that near-field ethene:methanol ratios track pyrolysis conditions and hence inform the abundance of other emitted VOCs. Finally, we apply CrIS ethene:methanol ratios to estimate the high-temperature pyrolysis fraction for the same plume ensemble; the resulting fraction correlates with fire radiative power in a manner not well-captured by models.

1. Introduction

Fire-emitted volatile organic compounds (VOCs) drive formation of ozone and secondary organic aerosols (SOA) (e.g.; Ahern et al., 2019; Alvarado et al, 2015; Alvarado and Prinn, 2009; Bourgeois et al., 2021; Brey and Fischer, 2016; Hatch et al., 2015; He et al., 2024; Jin et al., 2026; McClure and Jaffe, 2018; Palmo et al., 2025; Xu et al., 2021), with adverse effects on human and ecosystem health (Cascio et al., 2018; Reid et al., 2016; Fischer et al., 2018; Jaffe et al., 2008; O'Dell et al., 2021). These effects are expected to intensify in many regions as wildfire frequency, burned area, and season length increase (Feng et al., 2025; Jones et al., 2022; Brey et al., 2020). In-situ VOC observations in smoke plumes are sparse and typically capture only a subset of ambient burning conditions, compromising efforts to diagnose fire emissions and track the subsequent plume chemistry. Satellite-based VOC measurements from the Cross-track Infrared Sounder (CrIS; Wells et al., 2025) offer new constraints to help address this gap. Here we analyze CrIS observations of methanol, ethene, ethyne, and hydrogen cyanide in smoke plumes across the western U.S. during 2018 and 2019 to assess the information these data can provide on fire emission processes.

The amount and speciation of emitted VOCs are governed by the physical and chemical processes that occur during combustion and by the type of fuel being burned (Crutzen & Andreae, 1990; Lobert & Warnatz, 1993; Yokelson et al., 1996, 1997; Andreae & Merlet, 2001; Andreae, 2019; Akagi et al., 2011; Sekimoto et al., 2018, 2023). Relative emission rates for VOCs containing only carbon, hydrogen, and oxygen depend mainly on combustion conditions; those for VOCs containing nitrogen, sulfur, or halogens also vary strongly with the fuel concentration of those elements (Andreae & Merlet, 2001; Roberts et al., 2020). In both cases, the VOC emissions arise predominantly from pyrolysis of the long-chain polymers contained in biomass (Lobert and Warnatz, 1993; Yokelson et al., 1996, 1997). Pyrolysis happens concurrently with the processes of drying, flaming combustion, and smoldering; its contribution changes over the lifetime of a fire and affects the evolving VOC speciation. For example, Sekimoto et al. (2018, 2023) find based on a factor analysis of data for the western US that ~85% of the variability in pyrogenic VOC speciation can be explained by the relative importance of low- vs. high-temperature pyrolysis. If broadly applicable, this relationship creates an opportunity for more robust parameterizations of fire emissions.

Satellite-based thermal infrared (IR) observations offer valuable chemical information for understanding fire processes, testing emission estimates, and mapping smoke plume evolution. Such measurements enable detection of multiple wildfire-relevant species, and unlike measurements in the ultraviolet and visible (UV/Vis), they are minimally impacted by the fine aerosols present in smoke. In particular, Wells et al. (2025) have recently developed retrievals for methanol (CH_3OH), ethene (C_2H_4), hydrogen cyanide (HCN), and ethyne (C_2H_2) using space-borne radiance observations from CrIS. Methanol and ethene are among the top 10 wildfire-emitted non-methane VOCs, with ethyne and HCN also prominent among the top 15 (Permar et al., 2021). HCN is a widely-used fire tracer because it is among the most abundant N-containing pyrogenic emissions, with few additional sources (Andreae & Merlet, 2001). Enhancements of all four species have been detected in wildfire smoke by satellite-borne IR instruments (Clarisse et al., 2011; Alvarado et al., 2011; De Longeville et al., 2021; Wells et al., 2025), but the capabilities and challenges in using this space-based data for quantitative fire analyses have not yet been examined in detail.

https://doi.org/10.5194/egusphere-2026-1669
Preprint. Discussion started: 12 May 2026

In this study, we use thermal IR observations from CrIS to map the distributions of methanol, ethene, ethyne, and HCN across the western U.S. during the summers of 2018 and 2019. For each species, we quantify the importance of wildfire smoke in terms of its contribution to the total signals measured by CrIS. We combine radiative transfer modeling with plume-specific analyses to explore the impacts of smoke altitude on thermal IR detection sensitivity, and show that by combining VOCs with similar vertical sensitivities we can quantify species:species enhancement ratios without requiring any plume height information. We then leverage these pyrogenic ratios to explore emission variability across individual fires and to assess processes controlling that variability. Our results provide a foundation to support more widespread use of thermal IR data in fire science applications.

2. Methods

2.1 CrIS trace gas retrievals

The CrIS instruments are a set of identical nadir-viewing Fourier Transform spectrometers flying on three sun-synchronous polar-orbiting satellites with nadir overpass times at ~01:30 and ~13:30 local time (LT): Suomi-NPP (launched 10/2011), JPSS-1/NOAA-20 (launched 11/2017), and JPSS-2/NOAA-21 (launched 11/2022). CrIS measures thermal IR radiances at high spectral resolution (0.625 cm^{-1}) with low noise (~0.04 K at 900 cm^{-1} and 280K) (Zavyalov et al., 2013) and has a 14 km nadir footprint. Analyses here employ daytime observations from CrIS onboard Suomi-NPP and focus on the western U.S. (30-50°N, 99-127°W) during the summers of 2018 (July 24 - September 13) and 2019 (July 22 - September 6); the specific timeframes match those for the airborne studies described in the next section.

The CrIS measurements of methanol, ethene, ethyne, and HCN employ the Retrieval of Organics from CrIS Radiances (ROCRv2) methodology described by Wells et al. (2025). Detection is based on the hyperspectral range index (HRI), a dimensionless quantity that quantifies the spectral signal for a given atmospheric species (Walker et al., 2011). HRIs for VOCs targeted here are derived over spectral ranges that encompass the ν_8 methanol absorption feature (C-O stretch; 1020-1040 cm^{-1}), the ν_7 ethene feature (=CH_2 wag; 940-960 cm^{-1}), the ν_5 ethyne feature (C-H bend, 720-740 cm^{-1}), and the ν_2 HCN feature (H-C-N bend, 700-720 cm^{-1}). VOC column abundances are then quantified using an artificial neural network (ANN) retrieval that is trained using synthetic HRIs generated by the Line-By-Line Radiative Transfer Model (LBLRTMv12.13; Clough et al., 2005; Wells et al., 2025).

Relevant predictors for the trained ANN include, along with the CrIS-measured HRIs, variables describing the atmospheric state (e.g., H_2O column, surface pressure, skin and atmospheric temperatures). Since thermal IR sensitivity depends on the thermal contrast between the Earth's surface and the absorber, ROCRv2 includes an additional predictor (P_{90}) that quantifies the pressure below which 90% of the VOC column resides. The parameter is of particular importance for smoke analyses given the potential for plumes to be lofted above the planetary boundary layer and for subsequent altitude changes during transport. P_{90} is not known *a priori* and is normally prescribed using independent information (e.g., from a model or from independent observations); here, we use complementary pairs of observed VOCs to constrain this vertical dependence.

Analyses in this paper primarily employ single-footprint HRIs and explore the vertical sensitivity of these signals using the P_{90} metric. We additionally use CrIS-measured carbon monoxide (CO; Worden et al., 2023; Kulawik and Payne 2025) as a fire tracer with an atmospheric lifetime far exceeding that of individual smoke plumes. This CrIS CO dataset was generated using the Tropospheric Ozone and Precursors for Earth System Sounding (TROPESS) processing system. Figure 1 illustrates the HRIs for methanol, ethene, ethyne, and HCN observed by CrIS in the Pole Creek fire plume on September 13, 2018 (Juncosa Calahorrano et al., 2021).

https://doi.org/10.5194/egusphere-2026-1669
Preprint. Discussion started: 12 May 2026

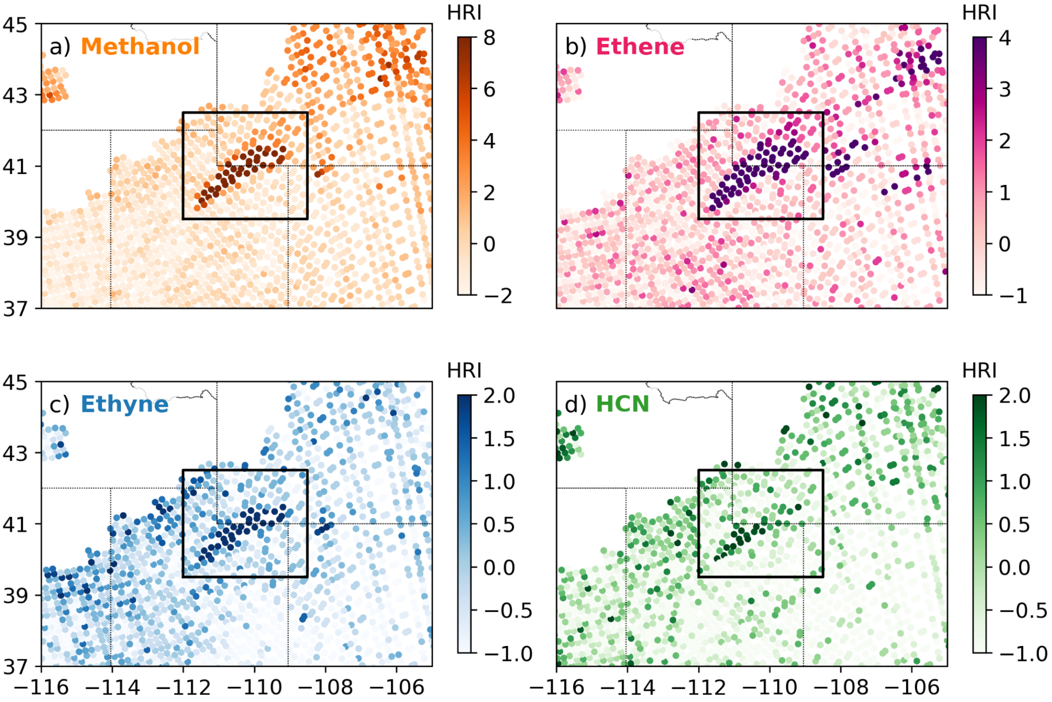

Figure 1. CrIS spectral detection of a) methanol, b) ethene, c) ethyne, and d) HCN in an individual fire plume. The hyperspectral range index (HRI) for each species is shown over a portion of the western U.S. on September 13, 2018, with the black box delineating the Pole Creek fire plume in Utah and Wyoming. Data gaps are due to clouds, which have been filtered out following Wells et al. (2020).

2.2 Airborne VOC observations in wildfire smoke plumes.

The 2018 Western Wildfire Experiment for Cloud Chemistry, Aerosol Absorption and Nitrogen (WE-CAN) (Lindaas et al., 2020; Juncosa Calahorrano et al., 2020; Permar et at., 2021) and the 2019 Fire Influence on Regional to Global Environments and Air Quality (FIREX-AQ) (Warneke et al., 2022) airborne campaigns characterized the chemical composition and evolution of biomass burning emissions over the western and southeastern U.S. WE-CAN (July 24 - September 13, 2018) employed the NSF C-130 and included flights out of Boise, ID (16 flights) and Broomsfield, CO (3 flights). FIREX-AQ employed the NASA DC-8 and consisted of two phases: the first (13 flights from July 22 - August 15, 2019) targeted western U.S. wildfires out of Boise, ID, and the second (7 flights from August 21 - 31, 2019) targeted smaller fires in the

https://doi.org/10.5194/egusphere-2026-1669
Preprint. Discussion started: 12 May 2026

southeastern U.S. out of Salida, KS. Analyses here utilize data from WE-CAN and from the western portion of FIREX-AQ.

WE-CAN and FIREX-AQ featured VOC measurements using Proton-Transfer-Reaction Time-of-Flight Mass Spectrometers (PTR-ToF-MS) and Whole Air Samplers (WAS). The PTR-ToF-MS instruments enabled in-situ detection of VOCs with proton affinity higher than water and were operated at 1or higher Hz sampling frequency. The WAS systems collected canister samples for subsequent off-line analysis. The NCAR Advanced-WAS (AWAS, Andrews et al., 2016) was deployed during WE-CAN (< 30 s sampling time; up to 46 canisters per flight), while the NOAA-integrated WAS (iWAS) was deployed during FIREX-AQ (< 10 s sampling time; up to 72 canisters per flight). Airborne analyses here employ PTR-ToF-MS methanol observations and AWAS/iWAS ethene observations, with all data averaged over the WAS sampling times. Uncertainties are reported at ± 15% (total; WE-CAN) and ± 50% (total; FIREX-AQ) for methanol, and at 5%/<8% (accuracy/precision; WE-CAN) and 2%/5% (accuracy/precision; FIREX-AQ) for ethene. More information about these instrument systems and their configuration during WE-CAN/FIREX-AQ can be found in Permar et al. (2021) and Warneke et al. (2022).

2.3 Model description.

We use the GEOS-Chem chemical transport model version 14.3.0 (The International GEOS-Chem User Community, 2021) to interpret the space-based VOC observations. The simulations use GEOS-FP assimilated meteorological fields from the NASA Global Modeling and Assimilation Office (GMAO), and are performed on a 0.25° × 0.325° grid nested over the western U.S. (33°-52° N, 99° - 129°). The nested runs extend from July 1 - September 30 of 2018 and 2019, with initial and boundary conditions obtained from global simulations performed respectively at 4° × 5° and 2° × 2.5°. The model employs a hybrid-sigma vertical grid with 47 layers extending to 0.01 hPa (22 in the lowest 5 km), and uses a 5-minute transport time step and a 10-minute chemical time step (10 and 20 minutes for the global runs). Model output is averaged from 12:00 - 15:00 LT for comparison with CrIS.

GEOS-Chem includes detailed HO_x-NO_x-VOC-ozone-BrO_x chemistry coupled with aerosols. HCN is not a standard GEOS-Chem tracer and we include it here following Li et al. (2003; 2009). Emissions in GEOS-Chem are computed using the HEMCO module, which includes biogenic VOC emissions from MEGANv2.1 (Guenther et al., 2012; Hu et al., 2015) and anthropogenic emissions from the Community Emissions Data System (CEDSv2). Jin et al (2023) evaluated multiple biomass burning inventories against the WE-CAN/FIREX-AQ airborne datasets and obtained the best model/measurement agreement when using the Global Fire Assimilation System (GFAS; CAMS, 2022); we therefore use GFAS here in the implementation described by Jin et al (2023). GFAS provides daily-averaged emissions for 40 pyrogenic species by converting Fire Radiative Power (FRP) observations from the Moderate Resolution Imaging Spectroradiometer (MODIS; Justice et al., 2002; Giglio et al., 2003) into estimates of dry matter consumption; fluxes are then derived using literature-based emission factors (CAMS, 2022; Keiser et al., 2012). GFAS also includes a process-based parameterization of plume injection heights based on the heat and convective energy released from each fire (Latham et al., 1994). The mean altitude of maximum injection ("mami") and the plume top are derived using a plume-rise model that is based on MODIS FRP and atmospheric profiles of temperature, wind, and atmospheric humidity from the European Center for Medium-Range Weather Forecasts (ECMWF; Freitas 2007, 2010; Paugam et al., 2015; Remy et al., 2017). Within GEOS-Chem, GFAS distributes fire emissions uniformly from the surface to the "mami" altitude while accounting for model resolution as described by Jin et al. (2023).

2.4 Smoke selection criteria.

We use the CrIS CO and ethene measurements described earlier to define categories of smoke influence over the western U.S. Selection proceeds in two steps. We first impose a CO threshold (>150 ppb at 510 and 680 hPa; Fischer et al., 2018; Juncosa Calahorrano et al., 2021) to identify all scenes impacted by smoke during our study period. We then use the ethene observations to distinguish between dense and diluted smoke. Ethene is a good marker for this purpose because it is among the most abundant VOCs emitted from fires (Permar et al., 2021), and its short atmospheric lifetime (~6 h at $[OH] = 5 \times 10^6$ molec/cm^3; Atkinson et al., 2006) results in large near-source enhancements over a low background. That regional background differs between the two study years since 2018 was a far more active fire year (Jin et al., 2023), and we find that different ethene HRI thresholds are therefore needed to resolve dense smoke scenes in the two cases (7 for 2018; 2 for 2019).

Finally, we aggregate the dense smoke scenes into coherent individual plumes for process analysis. Aggregation employs the density-based spatial clustering of applications with noise (DBSCAN) algorithm from the Python scikit-learn library (Ester et al., 1996; Schubert et al., 2017). DBSCAN groups data points with a dense population of close neighbors and excludes as outliers those that lie too far from a cluster. The two arguments needed for the algorithm are the radius distance and the minimum number of samples, which are set here to 60 km and 5, respectively (Figure S1). We next use fire detections from the Visible Infrared Imaging Radiometer Suite (VIIRS) with 375 m nominal resolution onboard Suomi-NPP to manually select coherent, intact plumes directly associated with a specific fire; we exclude transported plumes whose source location could not be readily identified (Schroeder et al., 2014a). The above procedure yields a total of 134 dense smoke plumes (116 in summer 2018; 18 in summer 2019; Figure S2).

https://doi.org/10.5194/egusphere-2026-1669
Preprint. Discussion started: 12 May 2026

Results and discussion.

Section 3.1. Methanol, ethene, ethyne, and HCN spectral enhancements in western U.S smoke plumes.

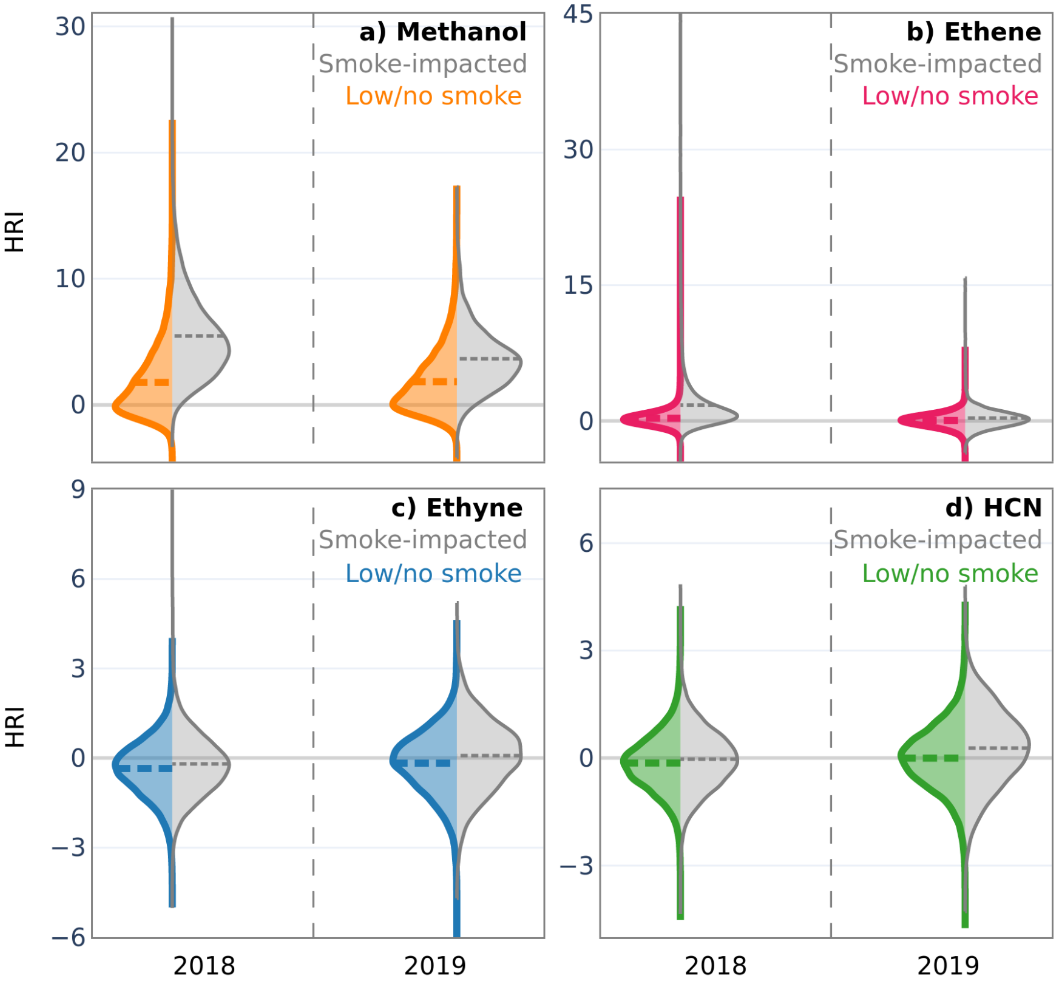

Figure 2. Distribution of VOC spectral signals in low/no-smoke and smoke-impacted scenes over the western U.S. as seen by CrIS during summers 2018 and 2019. Data reflect aggregated statistics at 0.5° × 0.5° horizontal resolution in low/no-smoke (color; N_{2018} = 38,214; N_{2019} = 27,848) and smoke-impacted (grey; N_{2018} = 29,782; N_{2019} = 3,694) scenes for a) methanol, b) ethene, c) ethyne, and d) HCN. Violin plots show the spread and the probability density of the data based on kernel density estimators. The dashed line shows the mean of the distribution in

https://doi.org/10.5194/egusphere-2026-1669
Preprint. Discussion started: 12 May 2026

each case. Smoke categories are defined based on CO as described in the text. Figure S3 shows violin plots for the single-footprint retrievals.

Figure 2 summarizes the distribution of CrIS-observed spectral signals (HRIs) for methanol, ethene, ethyne, and HCN inside versus outside of smoke-impacted areas of the western U.S. By construction, the HRI has a mean of zero and a standard deviation of one under background conditions (Walker et al., 2011) so that some negative values are seen in all cases. The highest spectral signal in smoke-free scenes is observed for methanol, reflecting its additional biogenic sources and longer lifetime, and its status as one of the most abundant VOCs in the atmosphere. All four VOCs reveal a clear impact from fires, with peak 0.5º × 0.5º HRI values in smoke ranging from 4.1 for HCN to 44 for ethene (peak single-footprint values range from 7.5 for HCN to 125 for ethene; Tables S1 and S2). For comparison, two past studies have used space-based data to quantify VOC HRIs in smoke plumes. De Longeville et al. (2021) report single-footprint values for the Infrared Atmospheric Sounder Interferometer (IASI) downwind of the 2020 Australian bushfires, with ethene HRIs exceeding 10 on four consecutive days. Wells et al. (2025) observed large VOC enhancements from the same Australian fires, with gridded CrIS HRI values (at 0.5° × 0.625°) >8 for methanol and ethyne and >4 for ethene and HCN. The specific HRI values vary with the spatial averaging approach and from instrument to instrument, as the signal depends strongly on the noise characteristics of the sensor (Hu et al., 2025).

The comparisons in Figure 2 also reveal larger peak smoke enhancements in 2018 than in 2019 for all four VOCs. Peak in-smoke HRIs were 2-8× higher (Table S1) in the more active 2018 fire season, which saw 6.7 million acres burnt across the western U.S. (Northwest, Northern Rockies, Northern California, Southern California, Great Basin, Southwest, and Rocky Mountain regions) versus just 1.6 million in 2019 (NIFC, 2018, 2019), resulting in a factor of 8.5 difference in the estimated total fire VOC emissions between the 2 years (Jin et al., 2023). This year-to-year difference is also reflected a the larger number of reported large fires for the region (560 in 2018 vs. 395 in 2019). Large fires are defined as those that have burnt a minimum of 100 acres in timber and 300 in grass or brush type fuels (NIFC, 2018, 2019).

The peak spectral enhancements for methanol and ethene in smoke are much larger than those for ethyne and HCN (Figure 2). This order matches the speciation of fire emissions: methanol and ethene are among the top 10 pyrogenic VOCs, with emission factors for western U.S. ecosystems approximately five times those of ethyne and HCN (Burling et al., 2010, 2011; Gilman et al., 2015; Permar et al., 2021; Gkatzelis et al., 2024). However, spectroscopic effects also contribute to the observed HRI patterns. In particular, while the peak ethyne and HCN enhancements show clear impacts from fires, their mean in-smoke HRIs in 2018 are only modestly higher than the corresponding background values–in contrast to the situation for methanol and ethene (Table S1). In effect, some fire scenes exhibit strong spectral enhancements for all four VOCs, while others show strong enhancements for methanol and ethene but not for ethyne or HCN. The discrepancy arises because detection sensitivity varies with altitude to differing degrees among the four VOCs: this vertical dependence is particularly strong for ethyne and HCN because their absorption features lie near the 720 cm^{-1} CO_2 band. In the following section, we explore implications of these species-dependent vertical sensitivities for fire VOC analyses.

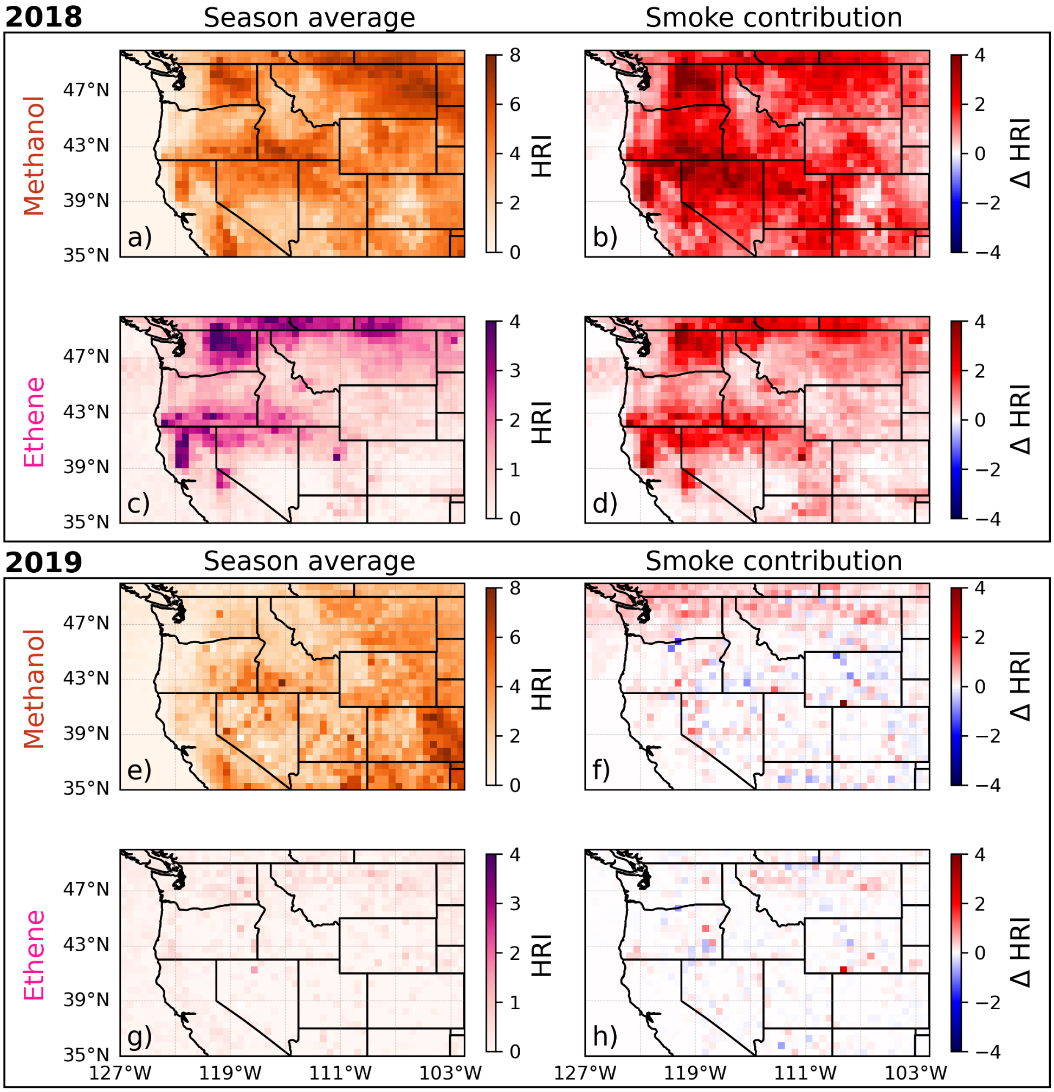

Figure 3. Spatial distribution of methanol and ethene spectral signals (HRIs) as measured by CrIS over the western U.S. during the summers of 2018 and 2019. The left column shows the seasonal-mean signals. The right column shows the contribution of smoke (ΔHRI) to the seasonal mean, quantified as the difference between the overall mean and the mean of all low/no smoke observations (Figures S4 and S5). Data are plotted on a 0.5° × 0.5° grid and span the WE-CAN (July 24 - September 13, 2018) and FIREX-AQ (July 26 - September 6, 2019) campaign timeframes.

https://doi.org/10.5194/egusphere-2026-1669
Preprint. Discussion started: 12 May 2026

Figure 3 maps the seasonally-averaged HRIs for methanol and ethene over the western U.S. during 2018/2019 campaign periods, and quantifies the contribution of smoke to that mean signal. Larger smoke enhancements are seen in 2018, showing that during active fire years pyrogenic VOCs are systematically elevated on a regional scale. These enhancements are strongest near and downwind of persistent fires (e.g., the Carr and Mendocino Fires in California) and are concentrated in the freshest portions of the plumes for ethene but more dispersed for methanol–reflecting its longer lifetime (~2.6 d vs. ~6 h at OH = 5 × 10^6 molec/cm^3, Atkinson et al., 2006). The California Central Valley exhibits large methanol signals in both years with minimal smoke contribution, revealing the presence of important non-pyrogenic sources such as dairy operations (e.g., Liu et al., 2022; Pfannerstill et al., 2023). The averaged spatial HRI and ΔHRI distributions for ethyne and HCN (Figure S4 and S5) are noisier than those of methanol and ethene. While ethyne and HCN enhancements are clearly seen for individual plumes (e.g., Figure 1), the impact of smoke on their seasonal-mean signals is less evident due to their lower emissions and weaker strength-of-signal.

3.2 Differences in thermal IR vertical sensitivity by compound

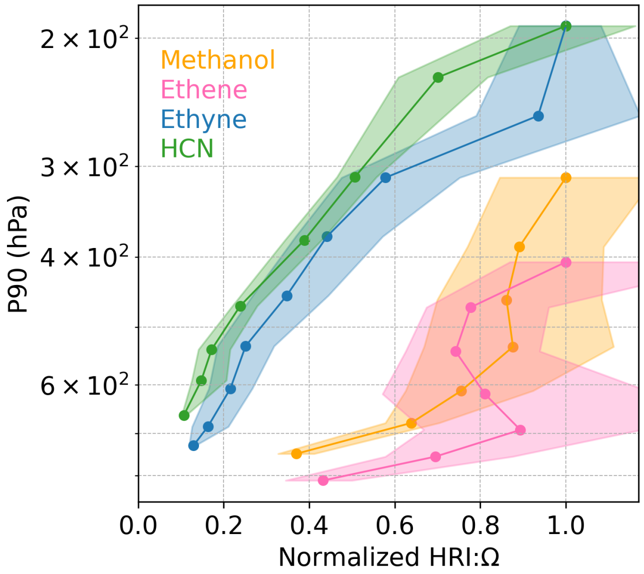

Figure 4. CrIS measurement sensitivity (expressed as the spectral signal to column ratio, HRI:Ω) as a function of the VOC's vertical location in the atmosphere. Data shown reflect model output

https://doi.org/10.5194/egusphere-2026-1669
Preprint. Discussion started: 12 May 2026

from GEOS-Chem/LBLRTM for smoky conditions in the western U.S. Results are shown for methanol, ethene, ethyne, and HCN as a function of P_{90}, the pressure below which 90% of the VOC column resides. Values are normalized to the peak sensitivity in each case, with lines and shading indicating the median and interquartile range for a given P_{90} bin.

Under typical conditions, the sensitivity of thermal IR measurements to a given VOC (i.e., the HRI:column ratio) increases with absorber altitude as the thermal contrast grows. Figure 4 quantifies this effect for our target VOCs based on synthetic data from LBLRTM. The plotted data are filtered to be representative of smoke-impacted areas in the western U.S. Specifically, we include only overland scenes where the water vapor column falls within the range of CrIS-observed values ($1.3 - 9.3 \times 10^{22}$ molecules cm^{-2}) over our analysis domain. We also impose a minimum HRI threshold that corresponds to the mean observed in-smoke values for methanol (5.0) and ethene (1.2), and that is prescribed at 2.0 for ethyne and HCN given the low mean HRIs for these species. Finally, we require that the VOC-specific P_{90} values are bracketed (in 30 hPa bins) by the range encountered in western U.S. fire plumes based on GEOS-Chem output for 2018 and 2019.

We see from Figure 4 that the vertical sensitivity dependence varies between compounds and is steeper for ethyne and HCN than it is for methanol and ethene, reflecting the CO_2 effect discussed earlier. It is also evident from Figure 4 that the strength of this dependence is quantitatively similar between i) methanol and ethene, and ii) ethyne and HCN. This pairwise similarity raises the possibility of leveraging specific VOC combinations to support fire analyses in a way that addresses key uncertainties related to plume height. Specifically, we hypothesize that VOC pairs with similar vertical sensitivity will exhibit spectral correlations that are conserved downwind regardless of the plume's vertical location. As the plume rises or subsides, the VOC:VOC spectral ratio for such pairs should not change significantly because the sensitivities of the two species are varying similarly. Changes to this ratio during downwind transport will then only occur in response to processes that alter the plume's chemical composition. On the other hand, the spectral correlation between pairs of VOCs with differing vertical sensitivities will change as the plume moves vertically. Such changes may provide information to constrain plume altitude changes during transport. In the following section, we test these ideas using case-study observations from the Pole Creek Fire plume.

3.3. Impact of plume altitude on VOC:VOC spectral ratios: the Pole Creek Plume.

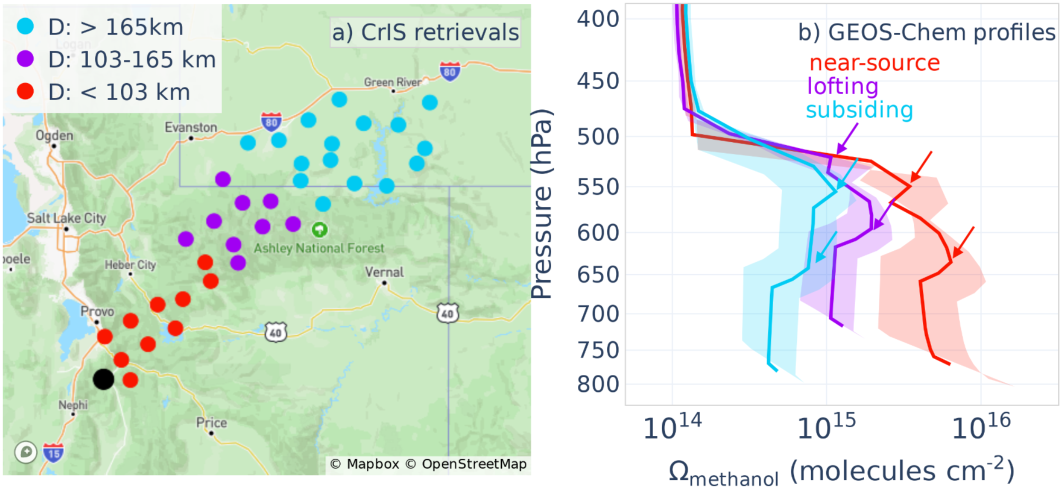

Figure 5. Plume transport and vertical displacement downwind of the Pole Creek Fire. a) CrIS measurement locations within the Pole Creek Fire plume on September 13, 2018, grouped by distance (D) from the fire centroid. The black dot shows the location of the VIIRS fire detection at the source. b) Mean in-plume methanol profiles at the CrIS overpass time as simulated by GEOS-Chem for the distance categories shown in panel a.

Biomass burning emissions rise vertically to an extent that depends on fire dynamics and on the atmosphere's thermal stratification (Freitas et al., 2007, 2010, Paugam et al., 2015; Remy et al., 2017). The resulting injection height is a highly uncertain model parameter and a focus of active research (June et al., 2025; Singh et al., 2025). After initial injection, topography and convection can lead to additional vertical displacement that further impacts the transport and fate of the plume. The September 2018 Pole Creek Fire in central Utah provides a well-defined case study for examining these processes (Juncosa Calahorrano et al., 2021). The lightning-initiated fire, located in the Wasatch Range near Provo, gave rise to a distinct and coherent plume that maintained its structure downwind with minimal influence from other regional sources. Clear enhancements of methanol, ethene, ethyne, and HCN are evident in the CrIS observations of this plume (Figure 1). Chemical transport model simulations and the regional topography (Figure 5) indicate that after initial injection, the plume was lofted orographically as it passed through the Uinta Mountains. The plume then subsided as it was transported past the Uinta Mountains and into southwest Wyoming.

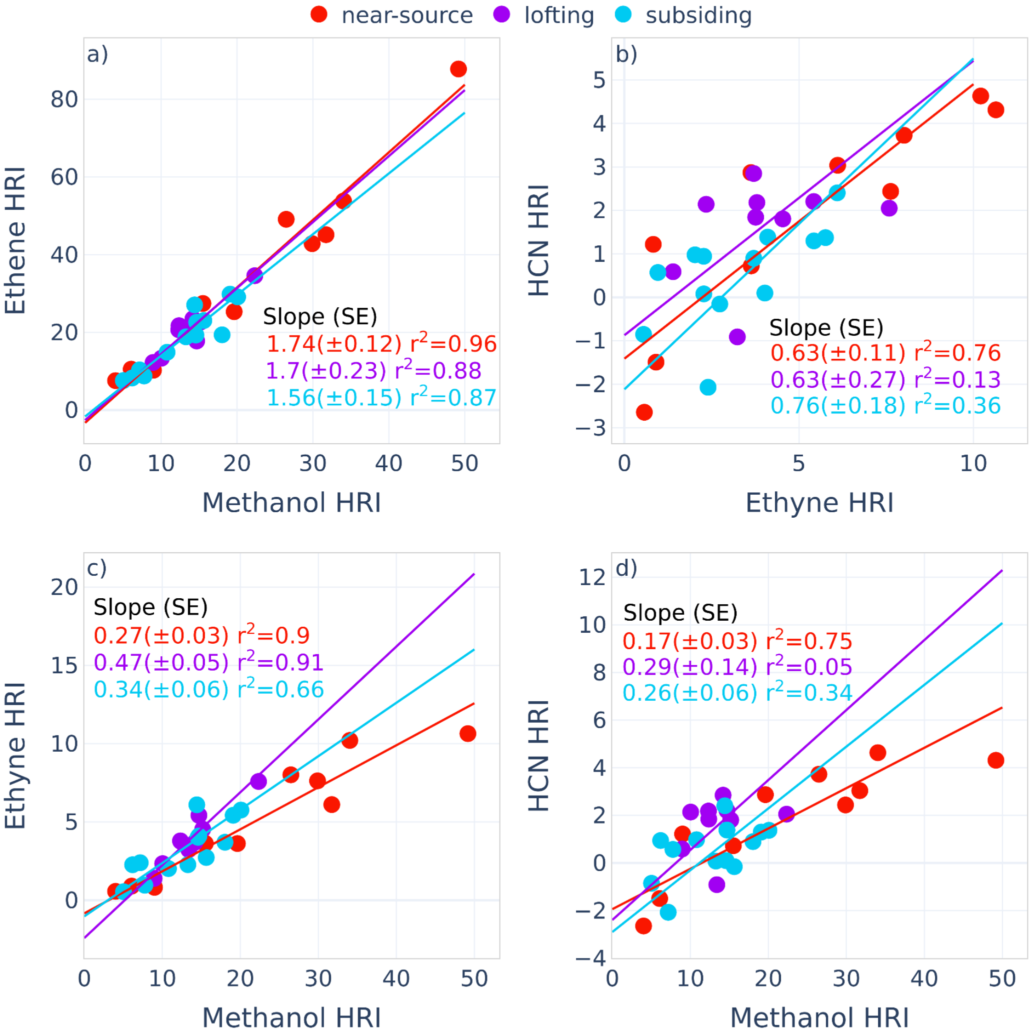

Figure 6. VOC spectral correlations as measured by CrIS in the Pole Creek Fire plume and as a function of downwind distance. The top row plots pairs of VOCs with similar vertical sensitivities; the slope of their spectral correlation does not statistically change with vertical

https://doi.org/10.5194/egusphere-2026-1669
Preprint. Discussion started: 12 May 2026

lofting. The bottom row shows pairs of VOCs with differing vertical sensitivities; here, the spectral signal for the VOC with more vertically-dependent sensitivity (plotted as the y-variable) is preferentially enhanced or suppressed as the plume is respectively displaced upward or downward. Distance categories reflect those shown in Figure 5. Slopes (with standard error) are calculated via Reduced Major Axis (RMA) regression.

Figure 6 plots the pairwise spectral correlations measured by CrIS for the four target VOCs within the Pole Creek Fire plume on September 13, 2018. The data are grouped by downwind distance and altitude as indicated in Figure 5. For methanol and ethene, with their similar vertical sensitivities, we observe a strong spectral correlation and a slope that is statistically independent of the plume's elevation. In fact, while the difference is not statistically significant, the lowest ethene:methanol slope is seen for the downwind population, which would be consistent with ethene oxidation over the ~4-5 h plume transport time (Juncosa Calahorrano et al., 2021). The same coherence holds for ethyne and HCN, the other VOC pair with similar vertical sensitivities, though with more scatter due to the weaker signal strength for these compounds. For such VOC pairs, the initial spectral slope at emission is thus unaffected by transport and will change only with the actual composition of the plume.

The situation is different for pairs of VOCs with divergent vertical sensitivities. Here, we expect the strength of the signal for the more vertically-sensitive compound (i.e., ethyne or HCN) to be preferentially enhanced as the plume rises and preferentially suppressed as the plume sinks. The VOC:VOC relationships plotted in Figure 6 (bottom row, with ethyne or HCN as the y-variable) are broadly consistent with this picture, with slopes that first increase as the plume is lifted over the Uinta Mountains, and then decrease as the plume subsides downwind. Chemical loss is not relevant in these cases given the corresponding oxidative lifetimes (from 2.3 d for ethyne to 74 d for HCN at OH = 5×10^6 molec/cm^3; (Atkinson et al., 2006)).

Species:species correlations are widely used in fire analyses to estimate emissions ratios with respect to a robust fire tracer (e.g., CO; Lindaas et al., 2020; Permar et al., 2021; Gkatzelis et al., 2024), to assess fire conditions and their evolution in time (Anderson et al., 2023), and to study downwind plume chemical evolution (Peng et al., 2020; Juncosa Calahorrano et al., 2020;

https://doi.org/10.5194/egusphere-2026-1669
Preprint. Discussion started: 12 May 2026

Lindaas et al., 2021; Jin et al., 2026). The findings above indicate that thermal IR spectral correlations between VOCs with different vertical sensitivities can help constrain plume altitude changes, while correlations between species with similar vertical sensitivities permit quantification of chemical ratios without requiring knowledge of the plume's vertical distribution. Below, we use CrIS observations to explore the second of these avenues with a focus on methanol and ethene.

3.4 Ethene:methanol column relationships in western U.S. wildfire plumes.

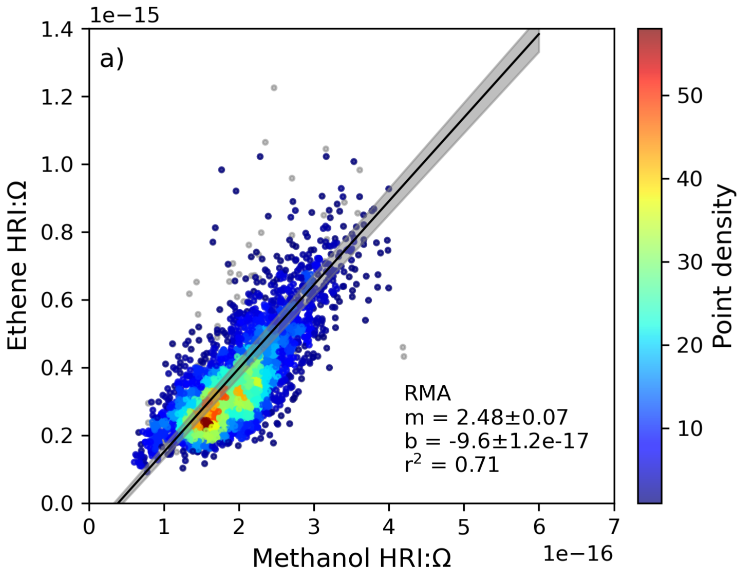

Figure 7. CrIS detection sensitivity for methanol versus ethene, plotted as the spectral signal to column ratio (HRI:Ω). Plotted values reflect synthetic data from the ROCRv2 training set, generated with LBLRTM based on randomized GEOS-Chem output. Data are filtered to reflect smoky conditions in the western U.S. and are colored by point density (N = 3090; 30 bins). RMA regression statistics with bootstrapped 95% confidence intervals are provided inset.

Quantifying VOC:VOC column enhancement ratios in smoke requires knowledge of their relative detection sensitivities–that is, their HRI:column (Ω) ratios. Figure 7 plots this quantity as computed by LBLRTM for methanol versus ethene, revealing the same close correlation (r^2 = 0.71) that was apparent in Figure 4. We can apply the corresponding slope as a conversion factor to directly translate CrIS-measured HRI:HRI enhancement ratios into column space for subsequent science analysis. For example, dividing the plume-wide Pole Creek methanol:ethene HRI slope of 1.73±0.06 by the sensitivity ratio from Figure 7 (2.48±0.04) yields an ethene:methanol column enhancement ratio of 0.70±0.03. The derivation requires no prior knowledge of the plume's vertical location and is thus not sensitive to uncertainties in plume injection height or to any subsequent altitude changes during transport. It also avoids relying on the neural-network retrieval used for global CrIS analyses (Wells et al., 2025), in which we find these extremely concentrated plume conditions are out-of-sample.

We next apply the above methodology to compute ethene:methanol column enhancement ratios for the set of dense wildfire plumes detected by CrIS over the western U.S. during the summer of 2018 and 2019. The analysis includes all plumes meeting the dense smoke criteria defined earlier along with the following requirements: i) > 4 CrIS observations; ii) ethene:methanol HRI correlation of $r^2 > 0.4$; iii) slope uncertainty < 80%; and iv) < 75 km from the fire source. The last requirement constrains the plume transport time to < 2.1 (±0.8) h at an average wind speed of 10 (±4) m s^{-1}, and is imposed to limit the impact of ethene oxidation on the derived ratios. In some of the cases outflow from 2-3 proximate fires merged into a single plume. When such sources were more than 100 km apart we considered them to be independent and applied the selection conditions separately to each one (some observational overlap is possible in this case). Outflow from fires less than 100 km apart was considered as a single plume, with the minimum possible downwind distance used in applying the near-source selection criterion. In this way we obtain a total of 67 plumes spanning 39 days during summer 2018, and 3 plumes spanning 3 days during summer 2019 (Figure 8a).

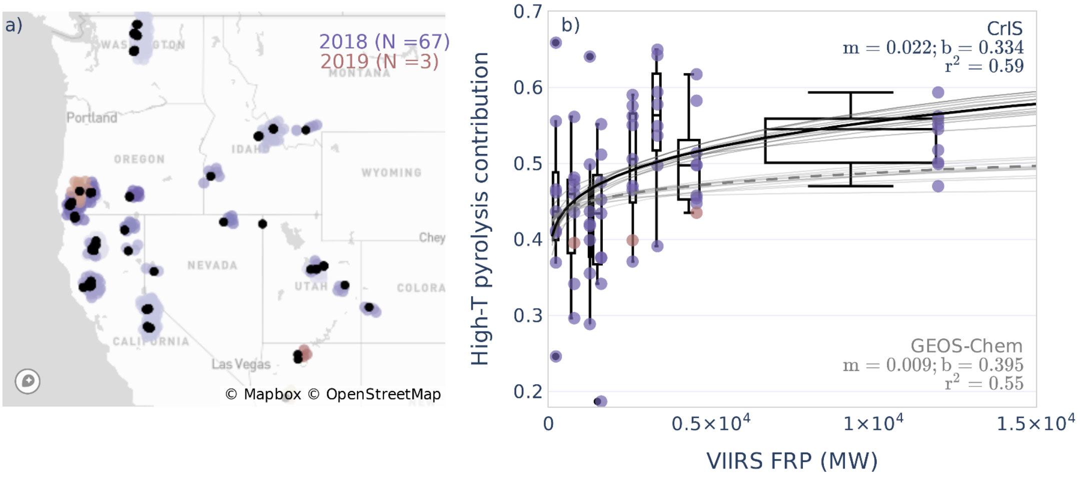

Figure 8. a) Fresh fire plumes detected by CrIS over the western U.S. during the summers of 2018 (67; purple) and 2019 (3; copper). Black dots show the averaged locations across all VIIRS detections of each fire. b) Contribution of high-temperature pyrolysis for each of these fire plumes (estimated from the CrIS ethene:methanol ratios as described in-text) as a function of VIIRS fire radiative power (FRP). Boxplots encompass the interquartile range (IQR) for each data bin; whiskers span data points within 1.5× IQR of the first and third quartiles. Boxplots are positioned at the bin-median FRPs with widths indicating the corresponding standard deviations. Lines of best fit with regression coefficients listed inset reflect a fourth-root power-law relationship and are calculated using the median high-temperature contribution and FRP for each bin. Thin grey lines show results from sensitivity analyses varying the plume selection criteria and number of analysis bins.

The CrIS-observed ethene:methanol column enhancement ratios for the 70 plumes have a mean value of 0.61 (standard deviation: ± 0.23), which is very similar to the mean GFAS emission ratio over this time and domain (0.63 ± 0.08; Figure S6). Both values are lower than the mean in-situ emission ratios across the ensemble of plumes sampled during the airborne WE-CAN (1.23±0.73; Permar et al., 2021) and FIREX-AQ (1.25±0.41; Gkatzelis et al., 2024) campaigns. A model test shows that in-situ pyrogenic ethene:methanol ratios can be directly compared to the corresponding total column enhancement ratios, and that both are expected to be similar to the underlying emission ratio (Figure S7). The comparison above thus indicates that the airborne sampling encountered plume conditions with higher ethene:methanol ratios than occur in the 70-plume CrIS dataset. The airborne sampling generally took place 2-4 hours after the CrIS overpass time, during the diel peak in fire activity and FRP (Wiggins et al., 2020); as will be seen below, higher ethene:methanol ratios are expected at that time. Both the airborne data and the CrIS observations also reveal a greater degree of ethene:methanol variability (standard deviations of 0.23-0.73) than would be predicted solely from the GFAS emission ratios (0.08).

Fuel type is traditionally the only variable considered when parameterizing fire VOC speciation in models and inventories (Andreae and Merlet , 2001; Akagi et al., 2011; Keiser et al., 2012; Andreae 2019). Dominant fuel types in the western U.S. include boreal and temperate forests, savannas, and cropland (Keiser et al., 2012), with reported ethene:methanol emission ratios of 0.53-0.70, 0.65 - 0.74, and 0.19 - 0.47, respectively (Andreae and Merlet , 2001; Akagi et al., 2011; Andreae 2019). The GFAS predictions for our analysis domain fall within that overall range, with fluxes mainly occurring at two discrete emission ratios of 0.61 and 0.66 (Figure S6). The larger spread seen in the spaceborne and in-situ observations points to other factors influencing pyrogenic VOC speciation within and between fuel types, and we investigate one such factor below.

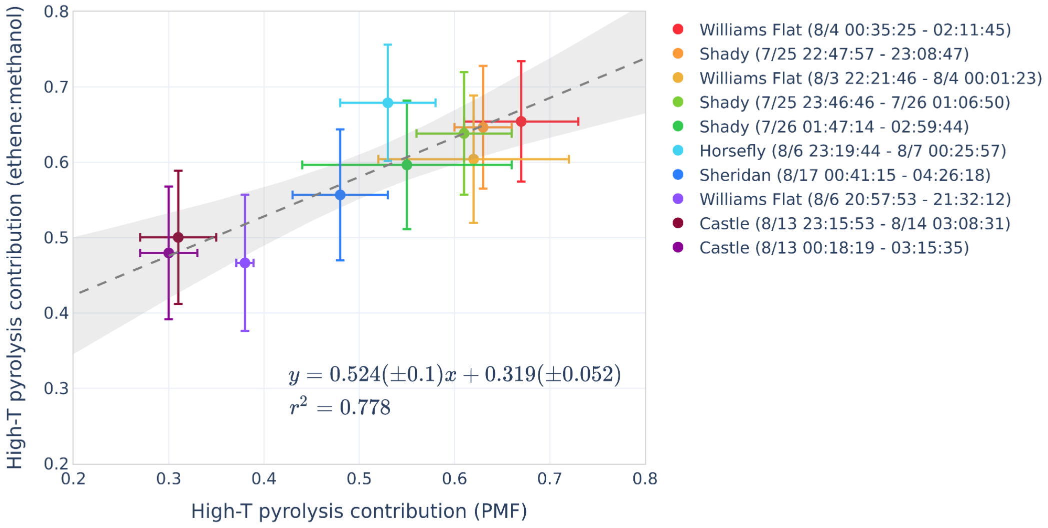

https://doi.org/10.5194/egusphere-2026-1669
Preprint. Discussion started: 12 May 2026

Figure 9. Fire pyrolysis conditions as inferred from FIREX-AQ airborne observations. High-temperature pyrolysis fractions derived from the in-plume ethene:methanol ratios (plotted as the y-variable) track the positive matrix factorization (PMF)-based estimates from Sekimoto et al. (2023) (plotted as the x-variable).

Recent analyses suggest that differences in pyrogenic VOC speciation arise mainly from distinct pyrolysis conditions. In particular, Sekimoto et al. (2018, 2023) found via positive matrix factorization (PMF) that 70-85% of the VOC variability across western U.S. fuels could be explained by two factors representing high-temperature and low-temperature pyrolysis processes. In effect, each factor is an averaged emission profile (ppb VOC/ppb total measured VOCs) that provides a fingerprint for high-T or low-T conditions across hundreds of VOCs. They further showed that these high-T versus low-T contributions can be estimated from the observed ratios of individual VOCs that are emitted under contrasting pyrolysis conditions (Eq. S1, S2). The example ratio they examined was that of ethyne (mainly a high-T product) to furan (low-T). However, neither compound is routinely observed outside of dedicated in-situ campaigns, and furan is very short-lived (~1 h at [OH] = 5 × 10^6 molec/cm^3; (IUPAC, 2024)), hindering broader application.

Ethene and methanol also have contrasting pyrolysis profiles, with ethene predominantly (72%) emitted under high-T conditions and methanol predominantly (62%) at low-T (Sekimoto et al., 2018). This complementarity, and the availability of space-based observations for both species, motivates us to explore the utility of the ethene:methanol pair for inferring high-T vs. low-T VOC emission contributions. Figure 9 tests this idea using airborne data from FIREX-AQ, comparing the high-T contribution as derived from in-plume ethene:methanol ratios (Eq. S2) to the Sekimoto et al. (2023) PMF-based results for their 10-plume dataset. The two estimates track each other closely (r^2 = 0.78), with a non-zero intercept that may reflect the limitations of a 2-species solution versus one based on hundreds of VOCs. Nevertheless, the comparison supports the idea that the ethene:methanol ratio is well-suited for characterizing the dominant thermal process occurring in fires–provided that observations are restricted to the near-field given ethene's ~6 h lifetime. We therefore extend the analysis above to the CrIS-observed ethene:methanol column enhancement ratios, which offer the opportunity for fire characterization that goes beyond the coverage of in-situ observations.

Figure 8b shows the high-T pyrolysis contributions derived from CrIS ethene:methanol column enhancement ratios for the population of fresh plumes (N=70) observed during the summers of 2018 and 2019 over the western U.S. Although these plumes were all measured at similar times of day and originate from similar fuel types, they exhibit a wide range of ethene:methanol ratios (0.15-1.28; Figure S8) and therefore of inferred high-T pyrolysis contributions (0.19-0.67). Data in Figure 8b are plotted as a function of VIIRS FRP, which as a measure of the energy released by a fire is proportional to the rate of fuel consumption and to the fourth power of absolute temperature (Wooster et al., 2003). Higher FRP values indicate more intense flaming and greater heat release, creating favorable conditions for high-T pyrolysis and therefore for a greater proportion of high-T VOCs (Sekimoto et al., 2023). For each fire we compute the corresponding FRP as the sum of all values within that fire scar for the corresponding CrIS measurement time; plumes with multiple fire sources then use the mean FRP across sources. We account for any bow-tie effects (Wolfe et al., 2013) by removing one observation from FRP pairs separated by < 375 m.

The high-T pyrolysis fractions inferred from the CrIS data increase with FRP at a rate of 0.022 (0.014 - 0.026) MW^{-1} with $r^2 = 0.59$ (0.35 - 0.71). Values in parentheses reflect the range across a suite of sensitivity tests varying the number of analysis bins (5-9) and the plume selection criteria (ethene:methanol HRI correlation threshold $r^2 = 0.4$-0.6; slope uncertainty 60-80%; maximum distance from source 50-125 km; fire separation distance 75-150 km). Results indicate that the observed relationship is statistically robust. Simulated results from GEOS-Chem (computed from the ethene:methanol column enhancement ratios in the same manner) show a similar correlation ($r^2 = 0.55$ [0.19 - 0.87]; Figure 8b) but a weaker slope (0.009 [0.002 - 0.012] MW^{-1}). While the magnitude of modeled emissions (and injection altitude) for any given fire is computed in GFAS as a function of FRP, the associated VOC speciation is based solely on fuel type without any explicit FRP dependence. The model correlation seen in Figures 8b and S8 thus arises solely from an association between fire FRP and vegetation fuel type. We propose that the model slope underestimate arises, at least in part, from the fact that higher FRP values also drive

https://doi.org/10.5194/egusphere-2026-1669
Preprint. Discussion started: 12 May 2026

enhanced high-T pyrolysis within individual vegetation categories, whereas GFAS (like other fire emission inventories) uses static emission factors for the entire fire life cycle.

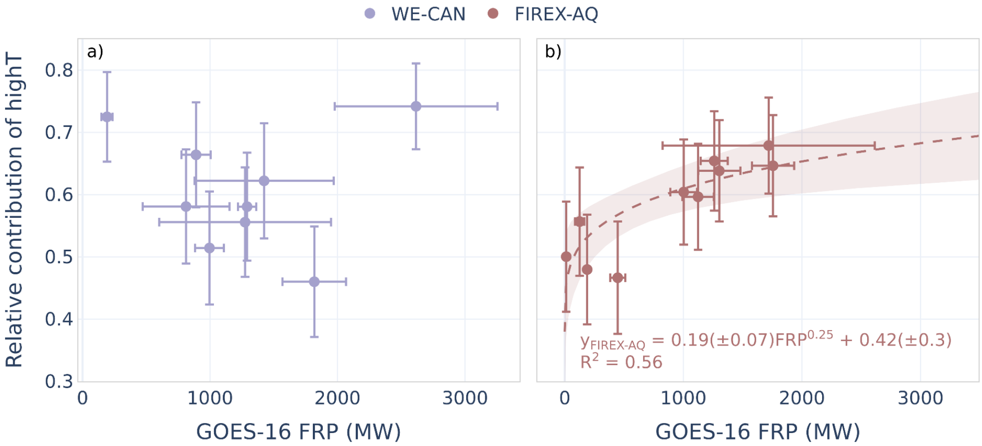

Figure 10. Fire pyrolysis conditions inferred from in-situ ethene:methanol observations as a function of FRP as measured by GOES West (GOES-16) in wildfire plumes over the western U.S. Plumes sampled during the a) 2018 WE-CAN campaign and b) 2019 FIREX-AQ campaign are shown.

Sekimoto et al. (2023) found a similarly strong correlation between their PMF-derived high-T pyrolysis contribution and FRP (from GOES-East and GOES-West) for their set of plumes sampled in-situ during FIREX-AQ. We find that this correlation is maintained when instead deriving the high-T contribution from in-situ ethene:methanol ratios (Figure 10b). However, the same coherence is not apparent in the WE-CAN in-situ data from the prior year. In particular, an analysis of the 9 WE-CAN plumes with < 4 h physical age featuring the most robust sampling (Permar et al., 2021) reveals no correlation between FRP and either the in-situ ethene:methanol ratios or the corresponding high-T pyrolysis fractions (Figure 10a). This WE-CAN comparison is restricted to FRP values from GOES-West since GEOS-East was not operational during summer 2018, and differences should also be expected with respect to the CrIS VIIRS-based analysis since FRP estimates differ between sensors (Li et al., 2018; 2020). Nevertheless, the WE-CAN FRP results appear at odds with the CrIS and FIREX-AQ findings. Possible explanations include the following: 1) the widespread regional smoke during the WE-CAN timeframe (Figure 3) may

https://doi.org/10.5194/egusphere-2026-1669
Preprint. Discussion started: 12 May 2026

affect the observed ethene:methanol ratios; 2) the more extensive smoke in 2018 could contribute to fire omission errors or to FRP underestimates (Schroeder et al., 2014b); 3) the sparser ethene observations during WE-CAN could prevent accurate diagnosis of the in-plume ethene:methanol ratios; or 4) the relationship between FRP, ethene:methanol, and pyrolysis conditions may be more variable than is apparent solely from the CrIS spaceborne and FIREX-AQ airborne data. More research is needed to clarify this issue and the broader utility of space-based ethene:methanol observations for fire process analysis.

4. Conclusions

Despite extensive research on wildfires, important uncertainties still exist regarding the chemical speciation of emitted compounds–including VOCs, which drive formation of aerosols and ozone. Satellite observations in the thermal IR provide new avenues for investigating the chemical properties of smoke, as they are sensitive to a variety of fire VOCs even in aerosol-rich plumes. Here, we analyzed CrIS observations of four pyrogenic VOCs (methanol, ethene, ethyne, HCN) in wildfire smoke over the western U.S during the summers of 2018 and 2019, corresponding respectively to the timeframes of the WE-CAN and FIREX-AQ airborne campaigns. We explored the use of such data for fire process studies, with particular focus on the impacts of vertically-dependent detection sensitivity and on leveraging species:species ratios to minimize plume-height uncertainties and diagnose fire properties.

The CrIS VOC spectral signals are strongly enhanced in wildfire smoke plumes, and these enhancements are larger for the more abundantly-emitted VOCs (i.e., methanol and ethene) and during more active fire seasons (i.e., 2018). Enhancements for shorter-lived VOCs can be used to identify fresh smoke, while those for longer-lived species map wider-range patterns of plume transport. Fires were widespread in 2018, and smoke impacts dominated the seasonal-mean spectral signals for the analyzed VOCs across the western U.S. The same did not occur in 2019, when there were far fewer fires. We find that thermal IR observations of ethene are well-suited for fire plume identification in both scenarios. As a short-lived pyrogenic VOC with low background concentrations it provides a clearer fingerprint of fresh smoke than do longer-lived tracers (e.g. CO, Lathem et al., 2013; Kloss et al., 2021; Arnold et al., 2025), while avoiding the need for manual visual analysis (e.g. NOAA Hazard Mapping System, Shen et al., 2026; Lee & Jaffe, 2024).

We show that fire-emitted VOCs with similar vertical sensitivities exhibit tight spectral (HRI:HRI) correlations that remain unchanged even if a plume changes altitude during transport. Plume injection heights are among the most uncertain parameters for wildfire modeling (Paugam et al., 2016): for instance, the GFAS inventory features observationally-informed plume height estimates, but recent studies find that a 1.7-2× increase in these values is needed to match regional and global aerosol observations (Singh et al., 2025; June et al., 2025). Findings here provide a methodology for deriving VOC:VOC column enhancement ratios from space-based data without requiring any information on plume height.

Conversely, for VOC pairs with differing vertical sensitivities, the HRI:HRI correlation changes in a coherent way as a function of plume altitude. Such VOC pairs could potentially be used to constrain near-source injection heights or subsequent plume altitude changes. A more detailed investigation of these effects, and their sensitivity to other factors (e.g., to any vertically-varying interferences) is needed to explore the broader viability of such an approach.
We next quantified ethene:methanol emission ratios across 70 western US fire plumes detected by CrIS during 2018 and 2019. The mean molar emission ratio measured by CrIS (0.61) is similar to the bottom-up prediction from GFAS (0.63) for the same region and time periods, but the satellite observations reveal a greater degree of variability than is present in the inventory (standard deviations of 0.23 vs. 0.08). The satellite-based emission ratios are lower than those reported by the WE-CAN and FIREX-AQ airborne field campaigns (~1.24); this difference may reflect the 2-4 h later in-situ sampling time, which coincides with peak fire intensity and likely with greater ethene:methanol emission ratios.

Finally, we present a satellite-based proxy approach for assessing the thermal conditions affecting fire VOC emissions. Specifically, we show that the relative importance of high- versus low-temperature pyrolysis conditions in a fire can be inferred from the in-plume ethene:methanol ratios. Pyrolysis fractions derived in this way correlate well with in-situ PMF-based results that are informed by hundreds of different VOCs (Sekimoto et al., 2018, 2023); space-borne ethene:methanol observations could therefore be broadly useful for constraining VOC speciation in wildfire plumes. We further demonstrate that high-T pyrolysis contributions derived from CrIS-observed ethene:methanol column enhancement ratios correlate with the fire radiative power (FRP) at the time of emission, as expected given the association between FRP and burn conditions that favor higher-T processes. Such a correlation also manifests in model predictions as a result of the association between FRP and fuel type; however, in that case the slope of the dependence is weaker and we suggest that this disparity reflects the fact that FRP also affects fire VOC speciation within individual ecosystem categories. A strong ethene:methanol vs. FRP correlation is apparent in airborne observations from the 2019 FIREX-AQ campaign, matching the CrIS findings, but the same is not true for the 2018 WE-CAN study which encountered widespread diluted smoke. The disparity underscores a need for additional analyses to understand drivers of VOC speciation under both fresh and aged smoke conditions.

Overall, these results demonstrate the utility of space-based VOC:VOC data for fire process analysis. A range of pyrogenic species with complementary chemical and detection properties are observable in the thermal IR. This opens opportunities for characterizing plume chemistry and transport, and for improving emission parameterizations in satellite-informed inventories (e.g., those using FRP). Findings here focus on the western U.S.; other sources of variability may play a role in different ecosystems, and additional research is needed to develop a more generalized understanding of fire VOC processes across different ecosystems and thermal regimes.

Data availability

The ROCRv2 VOC data used in this work are available at https://doi.org/10.13020/9r8x-pp66 (Wells et al., 2025). The single-footprint CrIS CO data used in this work are available at https://zenodo.org/records/17065859 (2018; Kulawik and Payne, 2025) and https://conservancy.umn.edu/items/c480f4b1-bb73-4612-81ac-388b468583dd (2019; Juncosa Calahorrano et al., 2026). The GEOS-Chem model code can be obtained at Zenodo https://doi.org/10.5281/zenodo.5711194. WE-CAN data is archived at https://data.eol.ucar.edu/master_lists/generated/we-can/. FIREX-AQ data is archived athttps://www-air.larc.nasa.gov/missions/firex-aq/ and at https://doi.org/10.5067/SUBORBITAL/FIREXAQ2019/DATA001 (FIREX-AQ science team, 2019). FRP data from VIIRS is available at https://doi.org/10.5067/FIRMS/VIIRS/VNP14IMGT_NRT.002 (NASA VIIRS Land Science Team, 2020).

Code availability

https://conservancy.umn.edu/items/c480f4b1-bb73-4612-81ac-388b468583dd (Juncosa Calahorrano et al., 2026)

Author contributions. Conceptualization: DBM and KCW. Data curation: JFJC, KCW, CH, VHP, WP, LH, APS, IK, EVF, VS, KS, AL, GG, JBG, MC, CW. Formal analysis: JFJC and DBM. Funding acquisition: DBM. Investigation: JFJC. Methodology: JFJC, DBM, KCW, CH, VHP, JFB. Project administration: DBM. Supervision: DBM. Writing (original draft preparation): JFJC and DBM. Writing (review and editing): all authors.

Competing interests

One of the co-authors is a member of the editorial board for Atmospheric Chemistry and Physics. The authors have no other competing interests to declare.

Financial support

This project was funded by NOAA (NA22OAR4310200) and NASA (Grant 80NSSC24M0037). Computing resources were provided by the Minnesota Supercomputing Institute at the University of Minnesota. Part of this work was carried out at the Jet Propulsion Laboratory, California Institute of Technology, under a contract with NASA (80NM0018D0004). Lu Hu and Wade Permar were supported by the NSF (AGS-2144896). Funding for the WE-CAN data collection was provided by the NSF (AGS-1650786, AGS-1650275, AGS-1950327, AGS-1748266, and AGS-1652688) and NOAA (NA17OAR4310010 and NA17OAR4310001).

Acknowledgement

We thank Wilfrid Schroeder, Louis Giglio, and Evan Ellicott for their insights and assistance with the use of the VIIRS FRP data. We also thank Susan Kulawik and the TROPESS team at JPL for their contributions to the CrIS CO data used in this work.

References.

Ahern, A. T., Robinson, E. S., Tkacik, D. S., Saleh, R., Hatch, L. E., Barsanti, K. C., Stockwell, C. E., Yokelson, R. J., Presto, A. A., Robinson, A. L., Sullivan, R. C., & Donahue, N. M. (2019). Production of Secondary Organic Aerosol During Aging of Biomass Burning Smoke From Fresh Fuels and Its Relationship to VOC Precursors. *Journal of Geophysical Research: Atmospheres*, *124*(6), 3583–3606. https://doi.org/10.1029/2018JD029068

Akagi, S. K., Yokelson, R. J., Wiedinmyer, C., Alvarado, M. J., Reid, J. S., Karl, T., Crounse, J. D., & Wennberg, P. O. (2011). Emission factors for open and domestic biomass burning for use in atmospheric models. *Atmospheric Chemistry and Physics*, *11*(9), 4039–4072. https://doi.org/10.5194/acp-11-4039-2011

Alvarado, M. J., Cady-Pereira, K. E., Xiao, Y., Millet, D. B., & Payne, V. H. (2011). Emission Ratios for Ammonia and Formic Acid and Observations of Peroxy Acetyl Nitrate (PAN) and Ethylene in Biomass Burning Smoke as Seen by the Tropospheric Emission Spectrometer (TES). *Atmosphere*, *2*(4), 633–654. https://doi.org/10.3390/atmos2040633

Alvarado, M. J., Lonsdale, C. R., Yokelson, R. J., Akagi, S. K., Coe, H., Craven, J. S., Fischer, E. V., McMeeking, G. R., Seinfeld, J. H., Soni, T., Taylor, J. W., Weise, D. R., & Wold, C. E. (2015). Investigating the links between ozone and organic aerosol chemistry in a biomass burning plume from a prescribed fire in California chaparral. *Atmospheric Chemistry and Physics*, *15*(12), 6667–6688. https://doi.org/10.5194/acp-15-6667-2015

Alvarado, M. J., & Prinn, R. G. (2009). Formation of ozone and growth of aerosols in young smoke plumes from biomass burning: 1. Lagrangian parcel studies. *Journal of Geophysical Research: Atmospheres*, *114*(D9), 2008JD011144. https://doi.org/10.1029/2008JD011144

https://doi.org/10.5194/egusphere-2026-1669
Preprint. Discussion started: 12 May 2026

Anderson, L. D., Dix, B., Schnell, J., Yokelson, R., Veefkind, J. P., Ahmadov, R., & De Gouw, J. (2023). Analyzing the Impact of Evolving Combustion Conditions on the Composition of Wildfire Emissions Using Satellite Data. *Geophysical Research Letters*, *50*(23), e2023GL105811. https://doi.org/10.1029/2023GL105811

Arnold, M. M., Saide, P. E., Miyazaki, K., Bowman, K. W., Schnell, J. L., Ahmadov, R., Chen, X., Wang, J., & Neyra-Nazarrett, O. A. (2025). Constraints on the modeled vertical distribution of smoke during the 2020 western US wildfires from satellite data. Npj Clean Air, 1(1), 37. https://doi.org/10.1038/s44407-025-00036-3

Andreae, M. O. (2019). Emission of trace gases and aerosols from biomass burning – an updated assessment. *Atmospheric Chemistry and Physics*, *19*(13), 8523–8546. https://doi.org/10.5194/acp-19-8523-2019

Andreae, M. O., & Merlet, P. (2001). Emission of trace gases and aerosols from biomass burning. *Global Biogeochemical Cycles*, *15*(4), 955–966. https://doi.org/10.1029/2000GB001382

Andrews, S. J., Carpenter, L. J., Apel, E. C., Atlas, E., Donets, V., Hopkins, J. R., Hornbrook, R. S., Lewis, A. C., Lidster, R. T., Lueb, R., Minaeian, J., Navarro, M., Punjabi, S., Riemer, D., & Schauffler, S. (2016). A comparison of very short lived halocarbon (VSLS) and DMS aircraft measurements in the tropical west Pacific from CAST, ATTREX and CONTRAST. *Atmospheric Measurement Techniques*, *9*(10), 5213–5225. https://doi.org/10.5194/amt-9-5213-2016

Kloss, C., Sellitto, P., Von Hobe, M., Berthet, G., Smale, D., Krysztofiak, G., Xue, C., Qiu, C., Jégou, F., Ouerghemmi, I., & Legras, B. (2021). Australian Fires 2019–2020: Tropospheric and Stratospheric Pollution Throughout the Whole Fire Season. Frontiers in Environmental Science, 9, 652024. https://doi.org/10.3389/fenvs.2021.652024

Atkinson, R., Baulch, D. L., Cox, R. A., Crowley, J. N., Hampson, R. F., Hynes, R. G., Jenkin, M. E., Rossi, M. J., Troe, J., & IUPAC Subcommittee. (2006). Evaluated kinetic and photochemical data for atmospheric chemistry: Volume II – gas phase reactions of organic species. *Atmospheric Chemistry and Physics*, *6*(11), 3625–4055. https://doi.org/10.5194/acp-6-3625-2006

Bourgeois, I., Peischl, J., Neuman, J. A., Brown, S. S., Thompson, C. R., Aikin, K. C., Allen, H. M., Angot, H., Apel, E. C., Baublitz, C. B., Brewer, J. F., Campuzano-Jost, P., Commane, R., Crounse, J. D., Daube, B. C., DiGangi, J. P., Diskin, G. S., Emmons, L. K., Fiore, A. M., … Ryerson, T. B. (2021). Large contribution of biomass burning emissions to ozone throughout the global remote troposphere. *Proceedings of the National Academy of Sciences*, *118*(52), e2109628118. https://doi.org/10.1073/pnas.2109628118

Brey, S. J., Barnes, E. A., Pierce, J. R., Swann, A. L. S., & Fischer, E. V. (2021). Past Variance and Future Projections of the Environmental Conditions Driving Western U.S. Summertime Wildfire Burn Area. *Earth's Future*, *9*(2), e2020EF001645. https://doi.org/10.1029/2020EF001645

Brey, S. J., & Fischer, E. V. (2016). Smoke in the City: How Often and Where Does Smoke Impact Summertime Ozone in the United States? *Environmental Science & Technology*, *50*(3), 1288–1294. https://doi.org/10.1021/acs.est.5b05218

Burling, I. R., Yokelson, R. J., Akagi, S. K., Urbanski, S. P., Wold, C. E., Griffith, D. W. T., Johnson, T. J., Reardon, J., & Weise, D. R. (2011). Airborne and ground-based measurements of the trace gases and particles emitted by prescribed fires in the United States. *Atmospheric Chemistry and Physics*, *11*(23), 12197–12216. https://doi.org/10.5194/acp-11-12197-2011

Burling, I. R., Yokelson, R. J., Griffith, D. W. T., Johnson, T. J., Veres, P., Roberts, J. M., Warneke, C., Urbanski, S. P., Reardon, J., Weise, D. R., Hao, W. M., & De Gouw, J. (2010). Laboratory measurements of trace gas emissions from biomass burning of fuel types from the southeastern and southwestern United States. *Atmospheric Chemistry and Physics*, *10*(22), 11115–11130. https://doi.org/10.5194/acp-10-11115-2010

Cascio, W. E. (2018). Wildland fire smoke and human health. *Science of The Total Environment*, *624*, 586–595. https://doi.org/10.1016/j.scitotenv.2017.12.086

Clarisse, L., R'Honi, Y., Coheur, P.-F., Hurtmans, D., & Clerbaux, C. (2011). Thermal infrared nadir observations of 24 atmospheric gases: TRACE GAS OBSERVATIONS FROM IASI. *Geophysical Research Letters*, *38*(10), n/a-n/a. https://doi.org/10.1029/2011GL047271

Clough, S. A., Shephard, M. W., Mlawer, E. J., Delamere, J. S., Iacono, M. J., Cady-Pereira, K., Boukabara, S., & Brown, P. D. (2005). Atmospheric radiative transfer modeling: A summary of the AER codes. *Journal of Quantitative Spectroscopy and Radiative Transfer*, *91*(2), 233–244. https://doi.org/10.1016/j.jqsrt.2004.05.058

Copernicus Atmosphere Monitoring Service (2022): CAMS global biomass burning emissions based on fire radiative power (GFAS). Copernicus Atmosphere Monitoring Service (CAMS) Atmosphere Data Store, DOI: 10.24381/a05253c7 (Accessed on DD-MMM-YYYY)

Crutzen, P. J., & Andreae, M. O. (1990). Biomass Burning in the Tropics: Impact on Atmospheric Chemistry and Biogeochemical Cycles. *Science*, *250*(4988), 1669–1678. https://doi.org/10.1126/science.250.4988.1669

De Longueville, H., Clarisse, L., Whitburn, S., Franco, B., Bauduin, S., Clerbaux, C., Camy-Peyret, C., & Coheur, P. (2021). Identification of Short and Long-Lived Atmospheric Trace Gases From IASI Space Observations. *Geophysical Research Letters*, *48*(5), e2020GL091742. https://doi.org/10.1029/2020GL091742

Ester, M., Kriegel, H.-P., Sander, J., & Xu, X. (1996). A density-based algorithm for discovering clusters in large spatial databases with noise. *Proceedings of the Second International Conference on Knowledge Discovery and Data Mining, KDD'96*, 226–231.

Feng, X., Mickley, L. J., Kaplan, J. O., Kelp, M., Li, Y., & Liu, T. (2025). Large role of anthropogenic climate change in driving smoke concentrations across the western United States from 1992 to 2020. *Proceedings of the National Academy of Sciences*, 122(49), e2421903122. https://doi.org/10.1073/pnas.2421903122

FIREX-AQ science team (2019). Fire influence on regional to global environments and air quality [Dataset]. NASA. https://doi.org/10.5067/SUBORBITAL/FIREXAQ2019/DATA001

Fischer, E. V., Zhu, L., Payne, V. H., Worden, J. R., Jiang, Z., Kulawik, S. S., Brey, S., Hecobian, A., Gombos, D., Cady-Pereira, K., & Flocke, F. (2018). Using TES retrievals to investigate PAN in North American biomass burning plumes. *Atmospheric Chemistry and Physics*, *18*(8), 5639–5653. https://doi.org/10.5194/acp-18-5639-2018

Freitas, S. R., Longo, K. M., Chatfield, R., Latham, D., Silva Dias, M. A. F., Andreae, M. O., Prins, E., Santos, J. C., Gielow, R., & Carvalho Jr., J. A. (2007). Including the sub-grid scale plume rise of vegetation fires in low resolution atmospheric transport models.

Atmospheric Chemistry and Physics, *7*(13), 3385–3398. https://doi.org/10.5194/acp-7-3385-2007

Freitas, S. R., Longo, K. M., Trentmann, J., & Latham, D. (2010). Technical Note: Sensitivity of 1-D smoke plume rise models to the inclusion of environmental wind drag. *Atmospheric Chemistry and Physics*, *10*(2), 585–594. https://doi.org/10.5194/acp-10-585-2010

Giglio, L., Descloitres, J., Justice, C. O., & Kaufman, Y. J. (2003). An Enhanced Contextual Fire Detection Algorithm for MODIS. *Remote Sensing of Environment*, *87*(2–3), 273–282. https://doi.org/10.1016/S0034-4257(03)00184-6

Gilman, J. B., Lerner, B. M., Kuster, W. C., Goldan, P. D., Warneke, C., Veres, P. R., Roberts, J. M., De Gouw, J. A., Burling, I. R., & Yokelson, R. J. (2015). Biomass burning emissions and potential air quality impacts of volatile organic compounds and other trace gases from fuels common in the US. *Atmospheric Chemistry and Physics*, *15*(24), 13915–13938. https://doi.org/10.5194/acp-15-13915-2015

Gkatzelis, G. I., Coggon, M. M., Stockwell, C. E., Hornbrook, R. S., Allen, H., Apel, E. C., Bela, M. M., Blake, D. R., Bourgeois, I., Brown, S. S., Campuzano-Jost, P., St. Clair, J. M., Crawford, J. H., Crounse, J. D., Day, D. A., DiGangi, J. P., Diskin, G. S., Fried, A., Gilman, J. B., … Warneke, C. (2024). Parameterizations of US wildfire and prescribed fire emission ratios and emission factors based on FIREX-AQ aircraft measurements. *Atmospheric Chemistry and Physics*, *24*(2), 929–956. https://doi.org/10.5194/acp-24-929-2024

Guenther, A. B., Jiang, X., Heald, C. L., Sakulyanontvittaya, T., Duhl, T., Emmons, L. K., & Wang, X. (2012). The Model of Emissions of Gases and Aerosols from Nature version 2.1 (MEGAN2.1): An extended and updated framework for modeling biogenic emissions. *Geoscientific Model Development*, *5*(6), 1471–1492. https://doi.org/10.5194/gmd-5-1471-2012

Hatch, L. E., Luo, W., Pankow, J. F., Yokelson, R. J., Stockwell, C. E., & Barsanti, K. C. (2015). Identification and quantification of gaseous organic compounds emitted from biomass burning using two-dimensional gas chromatography–time-of-flight mass spectrometry. *Atmospheric Chemistry and Physics*, *15*(4), 1865–1899. https://doi.org/10.5194/acp-15-1865-2015

He, Y., Zhao, B., Wang, S., Valorso, R., Chang, X., Yin, D., Feng, B., Camredon, M., Aumont, B., Dearden, A., Jathar, S. H., Shrivastava, M., Jiang, Z., Cappa, C. D., Yee, L. D., Seinfeld, J. H., Hao, J., & Donahue, N. M. (2024). Formation of secondary organic aerosol from wildfire emissions enhanced by long-time ageing. *Nature Geoscience*, *17*(2), 124–129. https://doi.org/10.1038/s41561-023-01355-4

Hu, C., Millet, D. B., Wells, K. C., Brewer, J. F., Juncosa Calahorrano, J. F., Payne, V. H., Taylor, J. K., & Tobin, D. C. (2026). First Aircraft-Based VOC Measurements Using Thermal Infrared Remote Sensing: Mapping Fire Plumes With the Scanning High-Resolution Interferometer Sounder (S-HIS). *Journal of Geophysical Research: Atmospheres*, *131*(4), e2025JD045605. https://doi.org/10.1029/2025JD045605

Hu, L., Millet, D. B., Baasandorj, M., Griffis, T. J., Turner, P., Helmig, D., Curtis, A. J., & Hueber, J. (2015). Isoprene emissions and impacts over an ecological transition region in the U.S. Upper Midwest inferred from tall tower measurements. *Journal of Geophysical Research: Atmospheres*, *120*(8), 3553–3571. https://doi.org/10.1002/2014JD022732

IUPAC Task Group on Atmospheric Chemical Kinetic Data Evaluation, https://iupac.aeris-data.fr/en/home/. This datasheet last evaluated: June 2024; last change in preferred values: June 2024.

Jaffe, D., Chand, D., Hafner, W., Westerling, A., & Spracklen, D. (2008). Influence of Fires on O_3 Concentrations in the Western U.S. *Environmental Science & Technology*, *42*(16), 5885–5891. https://doi.org/10.1021/es800084k

Jin, L., Permar, W., Selimovic, V., Ketcherside, D., Yokelson, R. J., Hornbrook, R. S., Apel, E. C., Ku, I.-T., Collett Jr., J. L., Sullivan, A. P., Jaffe, D. A., Pierce, J. R., Fried, A., Coggon, M. M., Gkatzelis, G. I., Warneke, C., Fischer, E. V., & Hu, L. (2023). Constraining emissions of volatile organic compounds from western US wildfires with WE-CAN and FIREX-AQ airborne observations. *Atmospheric Chemistry and Physics*, *23*(10), 5969–5991. https://doi.org/10.5194/acp-23-5969-2023

Jin, L., Coggon, M. M., Permar, W., Calahorrano, J. F. J., Palm, B. B., Gkatzelis, G. I., Robinson, M. A., Bourgeois, I., Hall, S. R., Peischl, J., Ullmann, K., Thornton, J. A., Warneke, C., Flocke, F., Fischer, E. V., Yokelson, R. J., & Hu, L. (2026). Ozone photochemistry in fresh biomass burning smoke over the United States. *Science AdvAnceS*.

Jones, M. W., Abatzoglou, J. T., Veraverbeke, S., Andela, N., Lasslop, G., Forkel, M., Smith, A. J. P., Burton, C., Betts, R. A., Van Der Werf, G. R., Sitch, S., Canadell, J. G., Santín, C., Kolden, C., Doerr, S. H., & Le Quéré, C. (2022). Global and Regional Trends and Drivers of Fire Under Climate Change. *Reviews of Geophysics*, *60*(3), e2020RG000726. https://doi.org/10.1029/2020RG000726

Juncosa Calahorrano, J. F., Lindaas, J., O'Dell, K., Palm, B. B., Peng, Q., Flocke, F., Pollack, I. B., Garofalo, L. A., Farmer, D. K., Pierce, J. R., Collett, J. L., Weinheimer, A., Campos, T., Hornbrook, R. S., Hall, S. R., Ullmann, K., Pothier, M. A., Apel, E. C., Permar, W., … Fischer, E. V. (2021). Daytime Oxidized Reactive Nitrogen Partitioning in Western U.S. Wildfire Smoke Plumes. *Journal of Geophysical Research: Atmospheres*, *126*(4), e2020JD033484. https://doi.org/10.1029/2020JD033484

Juncosa Calahorrano, J. F., Payne, V. H., Kulawik, S., Ford, B., Flocke, F., Campos, T., & Fischer, E. V. (2021). Evolution of Acyl Peroxynitrates (PANs) in Wildfire Smoke Plumes Detected by the Cross-Track Infrared Sounder (CrIS) Over the Western U.S. During Summer 2018. *Geophysical Research Letters*, *48*(23), e2021GL093405. https://doi.org/10.1029/2021GL093405

June, N. A., Ford, B., Croft, B., Chang, R. Y. -W., & Pierce, J. R. (2025). Inclusion of Biomass Burning Plume Injection Height in GEOS-Chem-TOMAS: Global-Scale Implications for Atmospheric Aerosols and Radiative Forcing. *Journal of Advances in Modeling Earth Systems*, *17*(6), e2024MS004849. https://doi.org/10.1029/2024MS004849

Justice, C. O., Giglio, L., Korontzi, S., Owens, J., Morisette, J. T., Roy, D., Descloitres, J., Alleaume, S., Petitcolin, F., & Kaufman, Y. (2002). The MODIS fire products. *Remote Sensing of Environment*, *83*(1–2), 244–262. https://doi.org/10.1016/S0034-4257(02)00076-7

Kaiser, J. W., Heil, A., Andreae, M. O., Benedetti, A., Chubarova, N., Jones, L., Morcrette, J.-J., Razinger, M., Schultz, M. G., Suttie, M., & Van Der Werf, G. R. (2012). Biomass burning emissions estimated with a global fire assimilation system based on observed fire radiative power. *Biogeosciences*, *9*(1), 527–554. https://doi.org/10.5194/bg-9-527-2012

Kulawik, S., & Payne, V. (2025). TROPESS WE-CAN CrIS-Suomi-NPP observations of PAN, CO, NH3, O3, CH3OH, Tatm, H2O, HDO, CH4 for Summer, 2018 over western USA (2025-09) [Data set]. Zenodo. https://doi.org/10.5281/zenodo.17065859.

Kloss, C., Sellitto, P., Von Hobe, M., Berthet, G., Smale, D., Krysztofiak, G., Xue, C., Qiu, C., Jégou, F., Ouerghemmi, I., & Legras, B. (2021). Australian Fires 2019–2020: Tropospheric and Stratospheric Pollution Throughout the Whole Fire Season. Frontiers in Environmental Science, 9, 652024. https://doi.org/10.3389/fenvs.2021.652024

Latham, D.: PLUMP: A one-dimensional plume predictor and cloud model for fire and smoke managers, General Technical Report INT-GTR-314, Intermountain Research Station, USDA Forest Service, Nov, 1994. https://www.fs.usda.gov/database/plump.htm

Lathem, T. L., Beyersdorf, A. J., Thornhill, K. L., Winstead, E. L., Cubison, M. J., Hecobian, A., Jimenez, J. L., Weber, R. J., Anderson, B. E., & Nenes, A. (2013). Analysis of CCN activity of Arctic aerosol and Canadian biomass burning during summer 2008. Atmospheric Chemistry and Physics, 13(5), 2735–2756. https://doi.org/10.5194/acp-13-2735-2013

Lee, H., & Jaffe, D. A. (2024). Wildfire Impacts on O3 in the Continental United States Using PM2.5 and a Generalized Additive Model (2018–2023). Environmental Science & Technology, 58(33), 14764–14774. https://doi.org/10.1021/acs.est.4c05870

Li, Q., Jacob, D. J., Yantosca, R. M., Heald, C. L., Singh, H. B., Koike, M., Zhao, Y., Sachse, G. W., & Streets, D. G. (2003). A global three-dimensional model analysis of the atmospheric budgets of HCN and CH_3 CN: Constraints from aircraft and ground measurements. *Journal of Geophysical Research: Atmospheres*, *108*(D21), 2002JD003075. https://doi.org/10.1029/2002JD003075

Li, Q., Palmer, P. I., Pumphrey, H. C., Bernath, P., & Mahieu, E. (2009). What drives the observed variability of HCN in the troposphere and lower stratosphere? *Atmospheric Chemistry and Physics*, *9*(21), 8531–8543. https://doi.org/10.5194/acp-9-8531-2009

Lindaas, J., Pollack, I. B., Calahorrano, J. J., O'Dell, K., Garofalo, L. A., Pothier, M. A., Farmer, D. K., Kreidenweis, S. M., Campos, T., Flocke, F., Weinheimer, A. J., Montzka, D. D., Tyndall, G. S., Apel, E. C., Hills, A. J., Hornbrook, R. S., Palm, B. B., Peng, Q., Thornton, J. A., … Fischer, E. V. (2021). Empirical Insights Into the Fate of Ammonia in Western U.S. Wildfire Smoke Plumes. *Journal of Geophysical Research: Atmospheres*, *126*(11), e2020JD033730. https://doi.org/10.1029/2020JD033730

Lindaas, J., Pollack, I. B., Garofalo, L. A., Pothier, M. A., Farmer, D. K., Kreidenweis, S. M., Campos, T. L., Flocke, F., Weinheimer, A. J., Montzka, D. D., Tyndall, G. S., Palm, B. B., Peng, Q., Thornton, J. A., Permar, W., Wielgasz, C., Hu, L., Ottmar, R. D., Restaino, J. C., … Fischer, E. V. (2020). Emissions of Reactive Nitrogen From Western U.S. Wildfires During Summer 2018. *Journal of Geophysical Research: Atmospheres*, *126*(2), e2020JD032657. https://doi.org/10.1029/2020JD032657

Liu, S., Barletta, B., Hornbrook, R. S., Fried, A., Peischl, J., Meinardi, S., Coggon, M., Lamplugh, A., Gilman, J. B., Gkatzelis, G. I., Warneke, C., Apel, E. C., Hills, A. J., Bourgeois, I., Walega, J., Weibring, P., Richter, D., Kuwayama, T., FitzGibbon, M., & Blake, D. (2022). Composition and reactivity of volatile organic compounds in the South Coast Air Basin and San Joaquin Valley of California. *Atmospheric Chemistry and Physics*, *22*(16), 10937–10954. https://doi.org/10.5194/acp-22-10937-2022

Lobert, J. M. and Warnatz, J.: Emissions from the combustion process in vegetation, in: Fire in the Environment: The Ecological, Atmospheric, and Climatic Importance of Vegetation Fires, edited by: Crutzen, P. J. and Goldammer, J. G., 15–37, J. Wiley & Sons, Chichester, UK, 1993.

McClure, C. D., & Jaffe, D. A. (2018). Investigation of high ozone events due to wildfire smoke in an urban area. *Atmospheric Environment*, *194*, 146–157. https://doi.org/10.1016/j.atmosenv.2018.09.021

National Interagency Coordination Center (NICC). 2018. Wildland Fire Summary and Statistics. Annual Report 2018. https://www.nifc.gov/sites/default/files/NICC/2-Predictive%20Services/Intelligence/Annual%20Reports/2018/annual_report_%202018_508.pdf. Access date December 7, 2025

National Interagency Coordination Center (NICC). 2019. Wildland Fire Summary and Statistics. Annual Report 2019 https://www.nifc.gov/sites/default/files/NICC/2-Predictive%20Services/Intelligence/Annual%20Reports/2019/annual_report_2019_508.pdf. Access date December 7, 2025

NASA VIIRS Land Science Team. (2020). VIIRS (S-NPP) I Band 375 m Active Fire Product NRT (Vector data) [Data set]. NASA LANCE MODIS at the MODAPS. https://doi.org/10.5067/FIRMS/VIIRS/VNP14IMGT_NRT.002 Date Accessed: 2025-03-13

O'Dell, K., Bilsback, K., Ford, B., Martenies, S. E., Magzamen, S., Fischer, E. V., & Pierce, J. R. (2021). Estimated Mortality and Morbidity Attributable to Smoke Plumes in the United States: Not Just a Western US Problem. *GeoHealth*, *5*(9), e2021GH000457. https://doi.org/10.1029/2021GH000457

Palmo, J. O., Heald, C. L., Blake, D. R., Bourgeois, I., Coggon, M., Collett, J., Flocke, F., Fried, A., Gkatzelis, G., Hall, S., Hu, L., Jimenez, J. L., Campuzano-Jost, P., Ku, I.-T., Nault, B., Palm, B., Peischl, J., Pollack, I., Sullivan, A., … Xu, L. (2025). Investigating fire-induced ozone production from local to global scales. *Atmospheric Chemistry and Physics*, *25*(22), 17107–17124. https://doi.org/10.5194/acp-25-17107-2025

Paugam, R., Wooster, M., Freitas, S., & Val Martin, M. (2016). A review of approaches to estimate wildfire plume injection height within large-scale atmospheric chemical transport models. *Atmospheric Chemistry and Physics*, *16*(2), 907–925. https://doi.org/10.5194/acp-16-907-2016

Peng, Q., Palm, B. B., Melander, K. E., Lee, B. H., Hall, S. R., Ullmann, K., Campos, T., Weinheimer, A. J., Apel, E. C., Hornbrook, R. S., Hills, A. J., Montzka, D. D., Flocke, F., Hu, L., Permar, W., Wielgasz, C., Lindaas, J., Pollack, I. B., Fischer, E. V., … Thornton, J. A. (2020). HONO Emissions from Western U.S. Wildfires Provide Dominant Radical Source in Fresh Wildfire Smoke. *Environmental Science & Technology*, *54*(10), 5954–5963. https://doi.org/10.1021/acs.est.0c00126

Permar, W., Wang, Q., Selimovic, V., Wielgasz, C., Yokelson, R. J., Hornbrook, R. S., Hills, A. J., Apel, E. C., Ku, I., Zhou, Y., Sive, B. C., Sullivan, A. P., Collett, J. L., Campos, T. L., Palm, B. B., Peng, Q., Thornton, J. A., Garofalo, L. A., Farmer, D. K., … Hu, L. (2021). Emissions of Trace Organic Gases From Western U.S. Wildfires Based on WE-CAN Aircraft Measurements. *Journal of Geophysical Research: Atmospheres*, *126*(11), e2020JD033838. https://doi.org/10.1029/2020JD033838

Pfannerstill, E. Y., Arata, C., Zhu, Q., Schulze, B. C., Woods, R., Seinfeld, J. H., Bucholtz, A., Cohen, R. C., & Goldstein, A. H. (2023). Volatile organic compound fluxes in the agricultural San Joaquin Valley – spatial distribution, source attribution, and inventory comparison. *Atmospheric Chemistry and Physics*, *23*(19), 12753–12780. https://doi.org/10.5194/acp-23-12753-2023

Reid, C. E., Jerrett, M., Tager, I. B., Petersen, M. L., Mann, J. K., & Balmes, J. R. (2016). Differential respiratory health effects from the 2008 northern California wildfires: A spatiotemporal approach. *Environmental Research*, *150*, 227–235. https://doi.org/10.1016/j.envres.2016.06.012

Rémy, S., Veira, A., Paugam, R., Sofiev, M., Kaiser, J. W., Marenco, F., Burton, S. P., Benedetti, A., Engelen, R. J., Ferrare, R., & Hair, J. W. (2017). Two global data sets of daily fire emission injection heights since 2003. *Atmospheric Chemistry and Physics*, *17*(4), 2921–2942. https://doi.org/10.5194/acp-17-2921-2017

Roberts, J. M., Stockwell, C. E., Yokelson, R. J., De Gouw, J., Liu, Y., Selimovic, V., Koss, A. R., Sekimoto, K., Coggon, M. M., Yuan, B., Zarzana, K. J., Brown, S. S., Santin, C., Doerr, S. H., & Warneke, C. (2020). The nitrogen budget of laboratory-simulated western US wildfires during the FIREX 2016 Fire Lab study. *Atmospheric Chemistry and Physics*, *20*(14), 8807–8826. https://doi.org/10.5194/acp-20-8807-2020

Schroeder, W., Oliva, P., Giglio, L., & Csiszar, I. A. (2014a). The New VIIRS 375 m active fire detection data product: Algorithm description and initial assessment. *Remote Sensing of Environment*, *143*, 85–96. https://doi.org/10.1016/j.rse.2013.12.008

Schroeder, W., Ellicott, E., Ichoku, C., Ellison, L., Dickinson, M. B., Ottmar, R. D., Clements, C., Hall, D., Ambrosia, V., & Kremens, R. (2014b). Integrated active fire retrievals and biomass burning emissions using complementary near-coincident ground, airborne and spaceborne sensor data. *Remote Sensing of Environment*, *140*, 719–730. https://doi.org/10.1016/j.rse.2013.10.010

Schubert, E., Sander, J., Ester, M., Kriegel, H. P., & Xu, X. (2017). DBSCAN Revisited, Revisited: Why and How You Should (Still) Use DBSCAN. *ACM Transactions on Database Systems*, *42*(3), 1–21. https://doi.org/10.1145/3068335

Sekimoto, K., Coggon, M. M., Gkatzelis, G. I., Stockwell, C. E., Peischl, J., Soja, A. J., & Warneke, C. (2023). Fuel-Type Independent Parameterization of Volatile Organic Compound Emissions from Western US Wildfires. *Environmental Science & Technology*, *57*(35), 13193–13204. https://doi.org/10.1021/acs.est.3c00537

https://doi.org/10.5194/egusphere-2026-1669
Preprint. Discussion started: 12 May 2026

Sekimoto, K., Koss, A. R., Gilman, J. B., Selimovic, V., Coggon, M. M., Zarzana, K. J., Yuan, B., Lerner, B. M., Brown, S. S., Warneke, C., Yokelson, R. J., Roberts, J. M., & De Gouw, J. (2018). High- and low-temperature pyrolysis profiles describe volatile organic compound emissions from western US wildfire fuels. *Atmospheric Chemistry and Physics*, *18*(13), 9263–9281. https://doi.org/10.5194/acp-18-9263-2018

Shen, J., Kaiser, J., & Jin, X. (2026). Fire-driven formaldehyde enhancement and population health burden revealed by TROPOMI in the contiguous U.S. Environmental Research Letters, 21(3), 034012. https://doi.org/10.1088/1748-9326/ae3788

Singh, I., Martin, R. V., Van Donkelaar, A., Li, C., Zhang, Y., Zhu, H., Zhang, D., & Lyapustin, A. (2025). Effects of Fire Plume Height on the Geophysical Estimation of Surface Fine Particulate Matter from Satellite Aerosol Optical Depth during North American Wildfires. *ACS ES&T Air*, *2*(10), 2071–2080. https://doi.org/10.1021/acsestair.5c00035

The International GEOS-Chem User Community. (2022). geoschem/GCClassic: GEOS-Chem Classic 14.0.0 (14.0.0). Zenodo. https://doi.org/10.5281/zenodo.7254984

Walker, J. C., Dudhia, A., & Carboni, E. (2011). An effective method for the detection of trace species demonstrated using the MetOp Infrared Atmospheric Sounding Interferometer. *Atmospheric Measurement Techniques*, *4*(8), 1567–1580. https://doi.org/10.5194/amt-4-1567-2011

Warneke, C., Schwarz, J. P., Dibb, J., Kalashnikova, O., Frost, G., Al-Saad, J., Brown, S. S., Brewer, Wm. A., Soja, A., Seidel, F. C., Washenfelder, R. A., Wiggins, E. B., Moore, R. H., Anderson, B. E., Jordan, C., Yacovitch, T. I., Herndon, S. C., Liu, S., Kuwayama, T., … The FIREX-AQ Science Team. (2023). Fire Influence on Regional to Global Environments and Air Quality (FIREX-AQ). *Journal of Geophysical Research: Atmospheres*, *128*(2), e2022JD037758. https://doi.org/10.1029/2022JD037758

Wells, K. C., Millet, D. B., Brewer, J. F., Payne, V. H., Cady-Pereira, K. E., Pernak, R., Kulawik, S., Vigouroux, C., Jones, N., Mahieu, E., Makarova, M., Nagahama, T., Ortega, I., Palm, M., Strong, K., Schneider, M., Smale, D., Sussmann, R., & Zhou, M. (2025). Global decadal measurements of methanol, ethene, ethyne, and HCN from the

Cross-track Infrared Sounder. *Atmospheric Measurement Techniques*, *18*(3), 695–716. https://doi.org/10.5194/amt-18-695-2025

Wells, K. C., Millet, D. B., and Brewer, J. F.: ROCRv2 methanol, ethene, ethyne, and HCN retrievals from the CrIS satellite sensor, Data Repository for the University of Minnesota (DRUM) [data set and code], https://doi.org/10.13020/9r8x-pp66, 2025.

Wiggins, E. B., Soja, A. J., Gargulinski, E., Halliday, H. S., Pierce, R. B., Schmidt, C. C., Nowak, J. B., DiGangi, J. P., Diskin, G. S., Katich, J. M., Perring, A. E., Schwarz, J. P., Anderson, B. E., Chen, G., Crosbie, E. C., Jordan, C., Robinson, C. E., Sanchez, K. J., Shingler, T. J., … Moore, R. H. (2020). High Temporal Resolution Satellite Observations of Fire Radiative Power Reveal Link Between Fire Behavior and Aerosol and Gas Emissions. *Geophysical Research Letters*, *47*(23), e2020GL090707. https://doi.org/10.1029/2020GL090707

Worden, H. M., Francis, G. L., Kulawik, S. S., Bowman, K. W., Cady-Pereira, K., Fu, D., Hegarty, J. D., Kantchev, V., Luo, M., Payne, V. H., Worden, J. R., Commane, R., & McKain, K. (2022). TROPESS/CrIS carbon monoxide profile validation with NOAA GML and ATom in situ aircraft observations. Atmospheric Measurement Techniques, 15(18), 5383–5398. https://doi.org/10.5194/amt-15-5383-2022

Wolfe, R. E., Lin, G., Nishihama, M., Tewari, K. P., Tilton, J. C., & Isaacman, A. R. (2013). Suomi NPP VIIRS prelaunch and on-orbit geometric calibration and characterization. *Journal of Geophysical Research: Atmospheres*, *118*(20). https://doi.org/10.1002/jgrd.50873

Wooster, M. J., Zhukov, B., & Oertel, D. (2003). Fire radiative energy for quantitative study of biomass burning: derivation from the BIRD experimental satellite and comparison to MODIS fire products. Remote Sensing of Environment, 86,83–107. https://doi.org/10.1016/S0034-4257(03)00070-1

Xu, L., Crounse, J. D., Vasquez, K. T., Allen, H., Wennberg, P. O., Bourgeois, I., Brown, S. S., Campuzano-Jost, P., Coggon, M. M., Crawford, J. H., DiGangi, J. P., Diskin, G. S., Fried, A., Gargulinski, E. M., Gilman, J. B., Gkatzelis, G. I., Guo, H., Hair, J. W., Hall, S. R., … Yokelson, R. J. (2021). Ozone chemistry in western U.S. wildfire plumes. *Science Advances*, *7*(50), eabl3648. https://doi.org/10.1126/sciadv.abl3648

Yokelson, R. J., Griffith, D. W. T., & Ward, D. E. (1996). Open-path Fourier transform infrared studies of large-scale laboratory biomass fires. *Journal of Geophysical Research: Atmospheres*, *101*(D15), 21067–21080. https://doi.org/10.1029/96JD01800

Yokelson, R. J., Susott, R., Ward, D. E., Reardon, J., & Griffith, D. W. T. (1997). Emissions from smoldering combustion of biomass measured by open-path Fourier transform infrared spectroscopy. *Journal of Geophysical Research: Atmospheres*, *102*(D15), 18865–18877. https://doi.org/10.1029/97JD00852